AD-A135 251 THE TWO DIMENSIONAL INEXTENSIBLE LIFTING MEMBRANE AIRFOIL - THEORY & EXPERIMENT(U) NAVAL AIR DEVELOPMENT CENTER WARMINSTER PA AIRCRAFT AND CREW S.. 1/1

UNCLASSIFIED S GREENHALGH 18 FEB 83 NADC-83096-60 F/G 20/4 NL

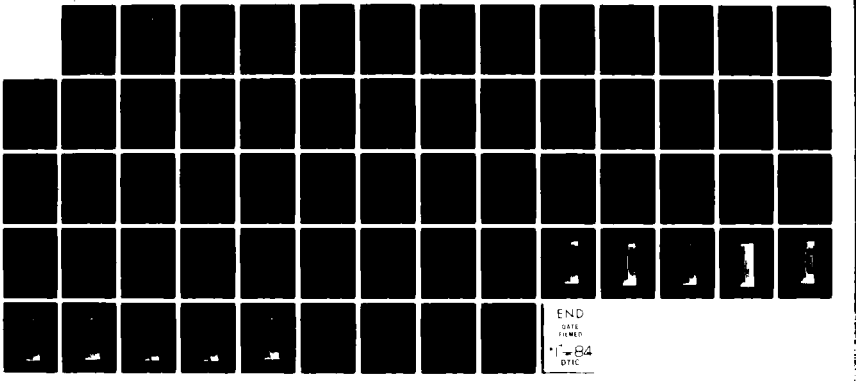

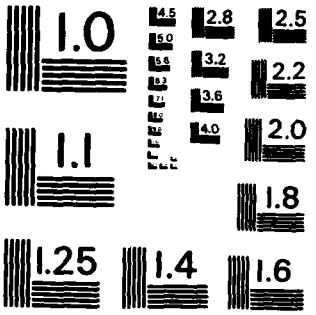

REPORT NO. NADC-83096-60

AD-A135 251

THE TWO DIMENSIONAL INEXTENSIBLE LIFTING MEMBRANE AIRFOIL - THEORY & EXPERIMENT

S. Greenhalgh
Aircraft and Crew Systems Technology Directorate
Naval Air Development Center
Warminster, PA 18974

18 February 1983

Final Report
IR No. GC123

APPROVED FOR PUBLIC RELEASE; DISTRUBUTION UNLIMITED

Prepared for
Naval Air Development Center
Department of the Navy
Warminster, PA 18974

DTIC FILE COPY

N O T I C E S

REPORT NUMBERING SYSTEM - The numbering of technical project reports issued by the Naval Air Development Center is arranged for specific identification purposes. Each number consists of the Center acronym, the calendar year in which the number was assigned, the sequence number of the report within the specific calendar year, and the official 2-digit correspondence code of the Command Office or the Functional Directorate responsible for the report. For example: Report No. NADC-78015-20 indicates the fifteenth Center report for the year 1978, and prepared by the Systems Directorate. The numerical codes are as follows:

CODE	OFFICE OR DIRECTORATE
00	Commander, Naval Air Development Center
01	Technical Director, Naval Air Development Center
02	Comptroller
10	Directorate Command Projects
20	Systems Directorate
30	Sensors & Avionics Technology Directorate
40	Communication & Navigation Technology Directorate
50	Software Computer Directorate
60	Aircraft & Crew Systems Technology Directorate
70	Planning Assessment Resources
80	Engineering Support Group

PRODUCT ENDORSEMENT - The discussion or instructions concerning commercial products herein do not constitute an endorsement by the Government nor do they convey or imply the license or right to use such products.

APPROVED BY: T. J. GALLAGHER
CAPT, MSC, USN

DATE: 15 August 1983

UNCLASSIFIED

SECURITY CLASSIFICATION OF THIS PAGE (When Data Entered)

REPORT DOCUMENTATION PAGE	READ INSTRUCTIONS BEFORE COMPLETING FORM
1. REPORT NUMBER: NADC-83096-60	2. GOVT ACCESSION NO.: A135251
3. RECIPIENT'S CATALOG NUMBER:	
4. TITLE (and Subtitle): The Two-Dimensional Inextensible Lifting Membrane Airfoil - Theory and Experiment	5. TYPE OF REPORT & PERIOD COVERED:
	6. PERFORMING ORG. REPORT NUMBER:
7. AUTHOR(s): S. Greenhalgh	8. CONTRACT OR GRANT NUMBER(s):
9. PERFORMING ORGANIZATION NAME AND ADDRESS: Naval Air Development Center, Aircraft & Crew Systems Technology Directorate, Warminster, PA 18974	10. PROGRAM ELEMENT, PROJECT, TASK AREA & WORK UNIT NUMBERS:
11. CONTROLLING OFFICE NAME AND ADDRESS: Naval Air Development Center, Warminster, PA 18974	12. REPORT DATE: 18 February 1983
	13. NUMBER OF PAGES: 64
14. MONITORING AGENCY NAME & ADDRESS (if different from Controlling Office)	15. SECURITY CLASS. (of this report): UNCLASSIFIED
	15a. DECLASSIFICATION/DOWNGRADING SCHEDULE:

16. DISTRIBUTION STATEMENT (of this Report)

Approved for Public Release; Distribution Unlimited

17. DISTRIBUTION STATEMENT (of the abstract entered in Block 20, if different from Report)

18. SUPPLEMENTARY NOTES

19. KEY WORDS (Continue on reverse side if necessary and identify by block number)

Aerodynamics
Lifting Surfaces
Membranes
Fabric Wings
Membrane Structure

20. ABSTRACT (Continue on reverse side if necessary and identify by block number)

A theoretical solution to the aerodynamic/structural two-dimensional flexible lifting membrane has been developed. The solution predicts lift, membrane shape and excess material length as a function of the tension in the membrane and the angle of attack of the membrane. The method is simpler than existing solutions and the results are in agreement with experiment. Wind tunnel tests on two-dimensional lifting membranes have been conducted at Reynolds numbers of approximately 1.3×10^6. Basic aerodynamic data and membrane

DD FORM 1 JAN 73 1473 EDITION OF 1 NOV 65 IS OBSOLETE

S/N 0102-LF-014-6601

UNCLASSIFIED

SECURITY CLASSIFICATION OF THIS PAGE (When Data Entered)

tension data were obtained.

TABLE OF CONTENTS

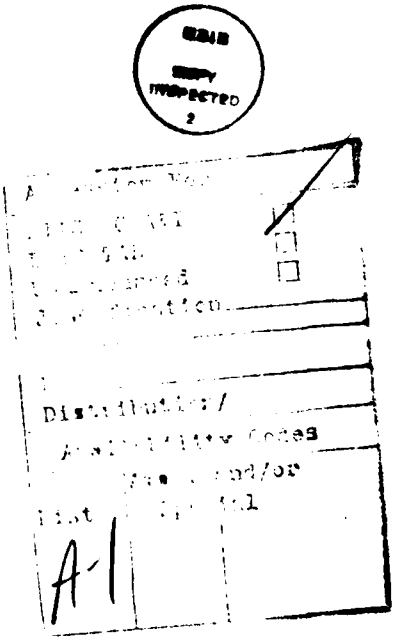

LIST OF FIGURES

LIST OF TABLES

LIST OF SYMBOLS

Symbol	Definition
$\{a\}$	column matrix with p elements, $\{a\} = \{0,0,0\ldots-p\alpha\}^T$
a_{ij}	aerodynamic influence coefficient, $a_{ij} = \frac{1}{1 + 2(i - j)}$
$[A]$	matrix of aerodynamic influence coefficients, $[A] = [a_{ij}]$
c	chord of airfoil, ft
$[C]$, $[E]$, $[H^*]$, $[G^*]$	matrices defined in Table I
C_ℓ	lift coefficient, $C_\ell = \frac{L}{\frac{1}{2}\rho U^2 c}$
C_T	tension coefficient, $C_T = \frac{T}{\frac{1}{2}\rho U^2 c}$
$[I]$	unit diagonal matrix
L	lift on airfoil per unit width, lbs/ft
ℓ	membrane length, ft
p	number of airfoil segments
T	tension in membrane per unit width, lbs/ft
U	freestream velocity, fps
$\bar{x}$	horizontal location on membrane, nondimensionalized by chord
XL	nondimensional membrane excess length, $XL = \frac{\ell - c}{c}$

L I S T O F S Y M B O L S (Continued)

Symbol	Definition
$\bar{y}$	vertical displacement of membrane, nondimensionalized by chord
$\bar{z}p\delta_i$	nondimensional curvature of element i, $(\frac{d^2\bar{y}}{d\bar{x}^2})$, $\delta_i = \frac{1}{2}(\theta_i - \theta_{i-1})$
α	airfoil angle of attack, rad
β_i	one-half nondimensional curvature of element i, $\beta_i = p\delta_i$
γ_i	average vortex sheet strength on element i, ft/sec, $\gamma_i = \frac{p}{c}\ \Gamma_i$
γ_i^*	nondimensional vortex sheet strength, $\gamma_i^* = \frac{\gamma_i}{U} = \hat{\Gamma}_p p$
Γ_i	line vortex strength on element i, ft^2/sec
$\hat{\Gamma}_i$	nondimensional vortex strength on element i, $\hat{\Gamma}_i = \frac{\hat{\Gamma}_i}{Uc}$
ΔC_{p_i}	pressure coefficient on element i, $\Delta C_{p_i} = \frac{\Delta p_i}{\rho \frac{U^2}{2}}$
Δp_i	pressure difference across element i, lbs/ft^2
θ_i	slope at trailing edge of element i
θ_i'	slope at trailing edge of element i, relative to freestream velocity direction
θ_{i-1}	slope at leading edge of element i
ρ	density of air, $slugs/ft^3$
ψ_i	average slope of element i, $(\frac{d\bar{y}}{d\bar{x}})$, $\psi_i = \frac{1}{2}(\theta_i + \theta_{i-1})$
ψ_i'	average slope of element i, relative to freestream velocity direction, $\psi_i' = \psi_i - \alpha$

SUMMARY

A study was conducted on the aerodynamic properties of a flexible, inextensible two-dimensional lifting membrane. Fabric wings have potential application to a variety of Naval vehicles including for example air launched torpedoes, high altitude RPV's, aerial targets, and ship launched decoys.

Flexible wings are potentially simple and inexpensive to manufacture and are capable of being folded and stored in a small space.

There are no known experimental results on the fundamental problem of a two-dimensional lifting surface. The two known theories by Thwaites and Neilson are complex and difficult to evaluate numerically. This study was intended as a fundamental research investigation to obtain an understanding of the basic physics of flow fields around two-dimensional flexible lifting surfaces. A linear mathematical model was developed.

A limited wind tunnel test program was conducted to obtain information to validate the theory. Comparison of theoretical and experimental results shows good agreement within five percent for a range of angles of attack from -5° to 8°. The combination of theoretical and experimental results accomplished the purpose of providing an improved understanding of the physics of this two-dimensional aero-structural problem.

This study is a summary of the first part of a two phase effort to investigate the aerodynamic characteristics of flexible membrane lifting surfaces. Phase two will investigate the three-dimensional lifting membrane.

THEORY FOR TWO-DIMENSIONAL MEMBRANE AIRFOIL

A theoretical procedure for calculating the lift, pressure distribution and shape of a two-dimensional airfoil whose lifting surface is a flexible inextensible membrane was developed and is described below.

The method consists of simultaneous solution of an aerodynamic equation describing the relationship between the vorticity distribution on a two-dimensional airfoil and the shape of the airfoil and a structural equation describing the relationship between the shape of the membrane and the loading on the membrane. The first equation is from thin-airfoil theory [1] and the second equation is obtained from a balance of forces on an element of the membrane. This second equation can also be viewed as the equation for the bending of a plate in the limiting case of zero flexural stiffness[2].

Together with these two equations there is an additional constraint which must be applied. In terms of the physical system, i.e., the manner in which the wind tunnel experiments were conducted, this constraint specifies the length of the flexible membrane. The only known theoretical solution to this formulation of the problem is found in the literature [3,4]. However, those solutions are complex since introduction of the length constraint makes the resulting set of governing equations non-linear. A simpler formulation can be obtained by applying a different constraint. As a consequence, the simultaneous solution of the aerodynamic and structural equations is obtained by solving a set of simultaneous linear algebraic equations, a much simpler task. Then, once the solution is obtained, the length of the membrane can be directly calculated. These two approaches are depicted graphically in figure 1.

Following classical thin airfoil theory, the airfoil is modelled as a sheet of vorticity of unknown strength $\gamma(x)$. The vortex sheet strength is determined by the condition that there is no flow through the airfoil. The camber of the airfoil is assumed to be small such that this boundary condition can be applied on the x-axis rather than on the airfoil itself[1]. From the geometry shown in figure 2, this relationship is:

$$\alpha + \frac{dy}{dx} = \frac{1}{2\pi U} \int_0^c \frac{\gamma(\xi)\, d\xi}{\xi - x} \qquad (1)$$

The Kutta condition must also be applied to this equation. This condition sets the level of total circulation on the airfoil and can be expressed as:

$$\gamma(c) = 0 \qquad (2)$$

The pressure difference across the airfoil at any chordwise location can also be expressed in terms of the vortex sheet strength from the Kutta-Joukowski law,

$$\Delta p = \rho U \gamma(x) \qquad (3)$$

Balancing forces on an element of the airfoil also yields a relationship between the pressure difference, the curvature of the element and the tension in the membrane as sketched in Figure 3.

$$\Delta p = - T \frac{d^2y}{dx^2} \tag{4}$$

This equation can be also derived from the one-dimensional plate bending equation when the flexural rigidity of the plate is assumed to be negligible, that is the bending moment in the plate is zero[2].

The final relationship which enters is the length of the membrane expressed in terms of chord length,

$$\frac{\ell}{c} = \frac{1}{c} \int_0^c \left[1 + \left(\frac{dy}{dx}\right)^2\right]^{1/2} dx = XL + 1 \tag{5}$$

XL is referred to as the excess length.

The tension in the membrane is assumed to be constant, that is, the contribution of the shear or viscous aerodynamic forces on the membrane to the tension can be neglected.

Integration of equation (3) gives the expression for the lift on the membrane.

$$L = \int_0^c \Delta p dx = \int_0^c \rho U \gamma(x)\, dx \tag{6}$$

Since the tension is constant in the membrane, an alternate expression for the lift can be obtained from equation (4),

$$L = - T \left[\left.\frac{dy}{dx}\right|_c - \left.\frac{dy}{dx}\right|_0\right] \tag{7}$$

Equations (1), (3), (4), and (5) taken with the boundary condition (2) can now be solved to determine the shape of the membrane, the vortex sheet strength and the pressure distribution on the membrane as well as the tension. This is the approach taken previously in the literature [3,4]. However, it is considerably simpler to specify the tension T, solve simultaneously equations (1), (3) and (4) with the boundary condition (2) and then determine the excess length from equation (5) (figure 1).

The governing equations can now be placed in a form suitable for solution on a digital computer. The membrane is broken up into p elements of length $\frac{c}{p}$, as shown in figure 4. The vortex sheet is represented by a concentrated line of strength Γ_i located at $\frac{1}{4}\ \frac{c}{p}$ from the leading edge of the element, and

the flow boundary condition is satisfied at a control point located at $\frac{3}{4}\frac{c}{p}$ from the leading edge of the element. It has been shown that taking this geometry for the aerodynamic element will inherently result in the Kutta condition (equation (2)) being satisfied as the number of elements becomes large [5]. Figure 4 then shows this geometry for development of the aerodynamic equation. The slope of each element is expressed in terms of an average slope defined in terms of the slope at the leading and trailing edges of the element (figure 3). The slope of element i is:

$$\psi_i = \frac{1}{2}(\theta_i + \theta_{i-1}) = \left.\frac{d\bar{y}}{d\bar{x}}\right|_i \qquad (8)$$

The non-dimensional curvature of the element is related to the slope change,

$$\delta_i = \frac{1}{2}(\theta_i - \theta_{i-1}) = \left.\frac{1}{2p}\frac{d^2\bar{y}}{d\bar{x}^2}\right|_i \qquad (9)$$

The vortex strength on the element is non-dimensionalized by the free-stream velocity and the chord.

$$\hat{\Gamma}_i = \frac{\Gamma_i}{Uc} \qquad (10)$$

This can be expressed in terms of a non-dimensional vortex sheet strength as:

$$\gamma_i^* = \hat{\Gamma}_i\, p \qquad (11)$$

The aerodynamic relationship (1) can then be expressed as,

$$\frac{\pi}{p}(\alpha - \psi_i) = \sum_{j=1}^{p} \frac{\hat{\Gamma}_j}{1 + 2(i - j)} \qquad (12)$$

Introducing an aerodynamic influence coefficient,

$$a_{ij} = \frac{1}{1 + 2(i - j)} \qquad (13)$$

$$\frac{\pi}{p}(\alpha - \psi_i) = a_{ij}\,\hat{\Gamma}_j \qquad (14)$$

Non-dimensionalizing equations (3) and (4) by introducing the pressure coefficient C_p, and the tension coefficient, C_T, yields:

$$(\Delta C_p)_i = 2\hat{\Gamma}_i\, p \qquad (15)$$

$$(\Delta C_p)_i = -2C_T\, p\, \delta_i \qquad (16)$$

Equations (15) and (16) can be combined to give:

$$\hat{\Gamma}_i = - C_T \delta_i \qquad (17)$$

Now equations (8), (9), (14), and (17) can be solved simultaneously with one additional condition that the trailing edge of the airfoil is on the x-axis. These equations can be written in matrix notation as,

$$[A] \quad \{\hat{\Gamma}_i\} = - \frac{\pi}{p} \{\psi_i - \alpha\} \qquad i = 1 \ldots p \qquad (18)$$

$$\{\hat{\Gamma}_i\} = - C_T \{\delta_i\} \qquad i = 1 \ldots p \qquad (19)$$

$$\sum_i \psi_i = 0 \qquad i = 1 \ldots p \qquad (20)$$

$$\{\psi_i\} = \frac{1}{2} [C] \{\theta_j\} \qquad \begin{matrix} i = 1 \ldots p \\ j = 0 \ldots p \end{matrix} \qquad (21)$$

$$\{\delta_i\} = - \frac{1}{2} [E] \{\theta_j\} \qquad \begin{matrix} i = 1 \ldots p \\ j = 0 \ldots p \end{matrix} \qquad (22)$$

There are 4p + 1 equations and 4p + 1 unknowns,

$\hat{\Gamma}_i, \delta_i, \psi_i$	3p unknowns
θ_j	p + 1 unknowns

It is convenient to define the average slope with respect to the freestream velocity:

$$\psi'_i = \psi_i - \alpha$$

$$\theta'_j = \theta_j - \alpha$$

Introducing these variables eliminates α from all equations except (20). We can also combine equations (20), (21) and (22) by eliminating θ_j and defining new matrices H* and G*, so that the set of equations is,

$$[A] \quad \{\hat{\Gamma}_i\} + \frac{\pi}{p} \{\psi'_i\} = 0 \qquad (23)$$

$$\{\hat{\Gamma}_i\} + C_T \{\delta_i\} = 0 \qquad (24)$$

$$[H^*] \{\psi'_i\} + [G^*]\{\delta_i\} = \{a\} \qquad (25)$$

H* and G* are now p x p matrices, and

$$\{a\} = \{0,0 \ldots\ldots, -p\alpha\}^T$$

The various matrices involved in these equations are given in Table I.

This set of equations can now be directly solved after choosing the number of segments, p, the angle of attack, α, and the tension coefficient, C_T. Then the pressure coefficient on the airfoil and the lift coefficient can be calculated from

$$\Delta C_{p_i} = 2\hat{\Gamma}_i \, p \tag{26}$$

and

$$C_\ell = \sum_{i=1}^{p} 2\hat{\Gamma}_i \tag{27}$$

As a check on the results, the lift coefficient can also be expressed from equation (7) as

$$C_\ell = -2 C_T \sum_{i=1}^{p} \delta_i$$

which can be written as

$$C_\ell = -C_T \left[(\psi_p + \delta_p) - (\psi_1 + \delta_1)\right] \tag{29}$$

The excess length can now be calculated from equation (5).

$$XL = \frac{1}{p} \sum_{i=1}^{p} \left[1 + \psi_i^2\right]^{1/2} - 1 \tag{30}$$

assuming that the slope is small

$$XL = \frac{1}{2p} \sum_{i=1}^{p} \psi_i^2 \tag{31}$$

In terms of the slope defined with respect to the freestream velocity,

$$\psi_i = \psi_i' + \alpha$$

recalling that

$$\sum_{i=1}^{p} \psi_i = 0$$

so that

$$\sum_{i=1}^{p} \psi_i' = -p\alpha$$

$$XL = \frac{1}{2p} \sum_{i=1}^{p} \psi_i'^2 - \frac{\alpha^2}{2} \tag{32}$$

The excess length is calculated from equation (32) after equations (23) through (25) have been solved. The approaches found in the literature consider the tension as unknown and proceed to solve equations (23) through (25) simultaneously with equation (32). This can be seen to be a much more complex approach as equation (32) is non-linear.

It is also possible to express equations (23) through (25) in an alternate form such that the unknown variables $\hat{\Gamma}_i$ and δ_i are replaced by variables which do not depend directly on the segment length. The rate at which the solution converges as the number of segments is increased can be readily determined. If we introduce:

$$\gamma_i^* = p\,\hat{\Gamma}_i$$

$$\beta_i = p\,\delta_i \tag{33}$$

Then the governing equations can be written as:

$$[A]\ \{\gamma_i^*\} + \pi\ \{\psi_i'\} = 0 \tag{34}$$

$$\{\gamma_i^*\} + C_T\ \{\beta_i\} = 0 \tag{35}$$

$$[H^*]\ \{\psi_i'\} + \frac{1}{p}\ [G^*]\ \{\beta_i\} = \{a\} \tag{36}$$

The number of segments now appears as a coefficient and γ_i^*, β_i, ψ_i depend only on the convergence rate.

One special case is of interest and that is the solution of this set of equations when the angle of attack is zero. In this case the set of equations becomes homogeneous and the value of C_T cannot be specified before hand. In this case it is convenient to combine these equations since finding specific values of C_T is equivalent to an eigenvalue problem. Equations (34) through (36) can be combined to yield the following equation,

$$\left[C_T\ [I] + \frac{\pi}{p}\ [H^*]^{-1}\ [G^*]\ [A]^{-1}\right] \{\psi_i'\} = -C_T\ [H^*]^{-1}\ \{a\} \tag{37}$$

Equation (37) is now expressed in such a form that the eigenvalues of C_T for the case in which $\alpha = 0$ can readily be calculated.

Calculations with these equations indicate that the solution converges relatively rapidly and that 20 segments are sufficient to obtain accurate results. With some experience with the equations it is quite straight-forward to find solutions for given values of the excess length corresponding to the manner in which the experiments were performed.

These equations were programmed with a numerical solution on a digital computer. Numerical solutions of the equations were evaluated for a range of angles of attack, excess lengths and tension coefficients.

Figures 5 through 19 are typical membrane shapes and aerodynamic data produced by the theory. Also shown on the figures is the predicted pressure distribution associated with the test condition. The parameter LAMDA Thwaites also shown on the figures is a non-dimensional parameter used by Thwaites[3] which is related to the membrane tension. LAMDA Thwaites is related to the tension coefficient, C_T, in the following way:

LAMDA Thwaites - $4/C_T$

EXPERIMENTS ON A TWO-DIMENSIONAL INEXTENSIBLE MEMBRANE AIRFOIL

Experimental data were obtained for several membranes over a range of excess material lengths corresponding to a practical range of angles of attack. (The "excess material length" of a membrane is defined as the difference between the length of the membrane and the chord expressed as a percentage of the chord length). Data were obtained from tests performed on a 12" wide x 18" long x 4 mil Mylar membrane in the Princeton two-dimensional tunnel. This tunnel possesses a 12" wide by 48" high test section.

Since there was no known previous experience in the testing of single surface fabric wings, prior to the testing some preliminary exploratory work was undertaken in the Princeton two-dimensional smoke tunnel to determine the sensitivity of the results to several of the more obvious physical variables, such as, material thickness, size of the membrane support rods, material porosity and the effects of side leakage. Although the smoke tunnel is a low Reynolds number facility, it proved to be useful in developing an understanding of the problem. Indeed, considerable practical information was obtained which assisted in the design of the final experimental apparatus. As a consequence of smoke tunnel tests on several 18" long membranes the following results were obtained:

a) Membrane Thickness - Experiment failed to reveal any discernible differences in behavior between a 1/2 mil Mylar membrane when compared to a 14 mil Mylar membrane. Indeed, several other non-porous materials possessing characteristics similar to Mylar were tested and the results of these tests were identical. Hence, membrane thickness was omitted in our considerations in the remainder of this study. However, this conclusion was only substantiated for material thickness to length ratios between 0.003% and 0.08%.

b) Leading Edge Radius - Leading edge supports of various radii were examined. Experimental results indicated that if the leading edge radius is less than 0.5 percent of the chord there was no measurable effect on the shape of the membrane or the flow about the leading edge of the membrane. This result

was obtained by comparison with the case in which the fabric alone provided the leading edge support.

c) Porosity - The porosity of the membrane material exhibited a large effect on the shape of the aerodynamically loaded membrane. Increasing the porosity of the material caused the point of maximum camber to move rearward toward the trailing edge of the system. Generally, for the woven materials that one would expect to employ in a lifting surface, i.e., dacron sail cloth, the system should exhibit virtually no porosity. Thus, it is not surprising that in the present set of tests, the last mentioned material acted in a non-porous manner.

d) Side Leakage - It was discovered that leakage about the side edges of the membrane had a considerable influence on the shape of the membrane. Therefore, a need for careful consideration of the side seal problem in the experimental design investigation was clearly demonstrated.

From theoretical considerations, discussed previously, it was important to insure that the tension developed within the membrane was measured in situ, i.e., while the membrane was subject to aerodynamic loading in the wind tunnel. A unique tension measuring system was developed that employed a strain gauge embedded in the membrane. For this system it was critically important that the neutral axis of the membrane and the strain gauge were coincident.

The experimental part of the present study considered the following parametric variations:

An 18" long by 12" wide by 4 mil piece of Mylar was employed to construct the membrane model. Experimental runs were performed with the Reynolds number in the range of 1.3×10^6. Excess material length was varied from 0.2% to 5.7% which induced a camber variation ranging from 3% to 15.5%. Finally, the physical arrangement of the wind tunnel during the experiments is shown in figure 20.

Data obtained from the experiments included lift, drag and membrane tension with all quantities measured as a function of the excess length and angle of attack.

Lift was calculated by utilizing the membrane induced pressure distribution on the tunnel floor and ceiling. Drag was ascertained from the momentum deficiency in the airfoil wake as measured with a drag rake. Tension was measured employing the strain gauge implanted in the membrane. The membrane was supported by two 1/2" x 1/8" elliptical rods which were free to rotate about their respective axes.

Figures 21 through 24 show some of the basic aerodynamic data obtained from our tests. In figure 21, we have recorded multiple plots of C_L vs α. Note that for the two separate sets of experiments dated 2/23/82 and 4/3/82, the second set of data were taken to broaden the base of the work, i.e., smaller excess lengths, and to confirm the characteristics of the lifting curve slope changes for the higher excess lengths. Observe that the theoretical flat plate lift line of 2π/radian is included on each plot to serve as a reference. The family of lift curves show that increasing the excess length of the membrane produces an

upward displacement of the lift curve. Such a result is consistent with aerodynamic theory since the larger the excess length the larger the airfoil camber. Hence, the vertical separation reflects the increase in the airfoil camber. It is also interesting to observe that membranes demonstrated a capability for producing positive lift at negative angles of attack for all the excess lengths tested. Flutter phenomena was observed under certain extreme conditions that could lead to vibration problems in design applications.

It is clear from results of the lift data secured during the runs of 23 February 1982 that when the excess lengths of the membrane are above XL = 1.69% there is a progressively decreasing lift curve slope above $\alpha = 0°$ for increases in the excess length. Flow visualization studies utilizing tufts, indicate that flow separation which is accompanied by small amplitude vibration is the cause of this fall off in the lift curve slope.

In general, the airfoils exhibit a benign stall behavior. For the greater excess lengths, in particular, increasing the angle of attack above 10° did not cause the lift to fall but rather it induced an increase in the aerodynamic drag.

This reflects a "self adjusting" feature whereby the point of maximum camber on the fabric wing moves forward increasing the lift on the leading edge portion of the wing as the region of separation on the trailing surface of the airfoil increases.

The benign stall behavior was demonstrated in the wind tunnel test for all excess lengths but high excess lengths are susceptible to dynamic problems and problems of separation and therefore, offer the least potential for design applications that require lift from increases of angle of attack.

Figure 22 shows a multiple plot of the drag force as a function of angle of attack with excess length as a parameter.

Coefficient of drag is a minimum at the zero angle of attack and increases nonlinearly for increasing or decreasing angles of attack. Also the larger the excess length, which implies larger airfoil camber, the larger the drag for a given angle of attack.

Coefficient of drag, C_d, is essentially a single valued function at zero angle of attack irrespective of excess length, this value is 0.015. Also the coefficient of drag vs angle of attack curve develops a pocket around the zero angle of attack where the drag rises more rapidly with angle of attack. The pocket in the drag curve narrows as the excess length increases indicating an increased sensitivity to angle of attack change as the excess length increases. This effect is especially noticeable for the XL = 5.69% membrane.

The experimental drag polars of figure 23 indicate that increasing excess length produces an increase in the lift. A limiting plateau is reached for the lift which depends on the value of the excess length and this limiting value is essentially constant as the drag increases. This is another representation of the benign stall behavior seen in the lift curves of figure 21.

Figure 24 shows the lift/drag ratios for the test runs of 23 February 1982. It is evident that the maximum lift/drag ratios occur near the zero angle of attack. However, the larger the excess length, the larger the lift to drag ratio for zero angle of attack. This result reflects the ability of camber to generate lift without producing drag. As the excess length of the membrane is decreased the curves broaden especially for angles of attack above zero, i.e., $\alpha > 0$, and the maximum lift/drag ratio falls by approximately 20%. The narrowness of the XL = 5.69% curve, i.e., the largest excess length tested, is evident. The large rise in lift/drag ratio is a consequence of the high lift produced by the large camber at zero angle of attack together with the low drag value. The sharpness of this curve is associated with the well defined narrow drag pocket around zero angle of attack associated with the high excess length.

The aerodynamic characteristics of the two-dimensional flexible inextensible airfoil compares favorably with solid surface sectional data over a similar angle of attack range at similar Reynolds numbers.

It should be noted that subsequent testing of a zero excess length membrane revealed an angularity of +1° associated with the tunnel air flow. The experimental data plots have been corrected to the true zero reference.

COMPARISON BETWEEN THEORY AND EXPERIMENT

Figure 25 is a comparison of the theoretical and experimental lift curve slopes for values of excess length, XL, of 0.21, 0.77, and 1.14. The comparison is remarkably good with differences less than approximately ±5% provided the angle of attack lies in the range of -5° to +8° and the excess lengths are confined to the values indicated. The theoretical curves on figure 25 can be represented by the following equation:

$$C_L = \frac{(2\pi)^2 \alpha^\circ}{360} + 0.726 (XL)^{\frac{1}{2}}$$

The equation was deduced from a log log plot of the data on figure 25.

From the above equation it is obvious that the lift produced by a two-dimensional flexible membrane exceeds the lift of a flat plate by an amount expressed approximately by $0.726\ (XL.)^{\frac{1}{2}}$. The lift is a nonlinear function of the excess length, XL, which is one of the main reasons for choosing tension rather than excess length as the independent variable in the theoretical solution.

In figure 26, we illustrate the comparison between the variation of the tension coefficient, C_T, as a function of α for both the experiments and the theoretical computations. The comparison is good and it is apparent that at the lower excess lengths the theoretical results are very good.

An empirical approximation to the theoretically derived coefficient of tension C_T vs α curves is as follows:

$$C_T = \frac{\alpha^\circ}{2\pi} (XL)^{-\frac{1}{2}} + 1.727$$

The equation was deduced from log log plots of the data on figure 26.

The value of the coefficient of tension, C_T corresponding to $\alpha = 0^\circ$, i.e., $C_T = 1.727$, may be shown to be an eigenvalue of the set of equations which we have formulated. The experimental data agrees with this theoretical conclusion. For this condition it is found that the shape of the membrane is symmetrical with respect to the mid-chord position, i.e. the maximum camber is located at the 50% chord position.

Under certain operating conditions the theory predicted the existence of two separate and distinct lift coefficients for the same angle of attack. The lift coefficient which was obtained depended upon whether the value of the tension coefficient, C_T, was greater than or less than the eigenvalue, i.e. $C_T = 1.727$. Therefore, it was possible to obtain positive lift corresponding to negative angles of attack and visa versa for tension coefficients below 1.727.

Note that the experimental results exhibited hysteresis loops when the excess length, XL >0. In particular an inflection point was found to develop in the membrane for the negative angles of attack. Further, when the angle of attack, $\alpha \geq 0^\circ$ the membrane possesses a convex shape; when the angle of attack $\alpha < 0^\circ$, a concave/convex shape developed.

It is evident that the prediction of two lift coefficients for a single angle of attack is the theoretical equivalent of the experimentally observed hysteresis phenomena. To assist in this comparison figures 27 to 36 are composite pictures of the theoretical and experimental membrane shapes where a computer developed membrane shape is superimposed over a wind tunnel photograph.

The theoretical overlay also contains computed data on the lift, tension, excess length and camber to be associated with a specific curve. Note that the coefficient of pressure, CP, is the theoretical pressure distribution. If the angle of attack $\alpha = 0$ the membrane shape possesses an inflection point located at the point where the coefficient of pressure equals zero. This can be seen from theoretical results, since the two-dimensional membrane equation indicates that the differential pressure across the membrane is directly proportional to the curvature of the membrane.

Comparison of the theoretical membrane shapes with the wind tunnel membrane shapes indicates good agreement over the range of values of excess length, XL, and angle of attack considered in these experiments.

Figures 37 and 38 represent plots of the coefficient of lift, C_L, and the coefficient of tension, C_T, as functions of the angle of attack. Comparison of the theoretical predictions with experimental hysteresis loops illustrates the close similarity of the results.

Observe that figure 39 is a sketch of the theoretically predicted coefficient of tension, C_T, as a function of excess length, XL, with angle of attack serving as a parameter. Near the C_T coordinate axis are a series of sketches of the theoretically predicted membrane shapes associated with different angles of attack for

a fixed excess length. These predicted shapes indicate that the point of maximum camber starts forward of the mid-chord point for high angles of attack and moves back to the mid-point as the angle of attack approaches zero. At the angle of attack $\alpha = 0°$ the membrane shape is symmetrical about the mid-cord point and the value of the coefficient of tension, C_T, is 1.727. As the angle of attack becomes negative, the value of coefficient of tension falls below 1.727, an inflection point develops near the leading edge of the membrane and the point of maximum camber moves from the center of the membrane towards the trailing edge. Theory indicates that for a given excess length there are several possible membrane configurations depending on the value of C_T. However, it is important to observe that each of these profiles possesses a different number of inflection points. In the event that the coefficient of tension, $C_T > 1.727$, there are no inflection points, and a single convex shape is produced. As the value of the coefficient of tension, C_T, is reduced, shapes with multiple inflection points develop. In practice the only membrane shapes observed are those with either zero or one inflection point. Further, is is noted that the membrane shapes with the one inflection point experience varying degrees of flutter.

Figure 39 is a sketch of a family of curves of theoretical coefficients of tension, C_T, vs the excess length, XL, with angle of attack serving as a parameter. The coefficient of tension, $C_T = 1.727$, is an eigenvalue and is the primary tension value associated with zero angle of attack. The tension coefficient of 0.902 is a line connecting the vertical tangency points of the angle of attack curves.

It can be seen from figure 39, i.e., the theoretical coefficient of tension, C_T, vs the excess length, XL, sketch, that hysteresis in the behavior of the system is to be expected. If we reduce the coefficient of tension, C_T, holding the excess length constant, it is impossible to reach certain negative angles of attack.

Assuming the membrane is moving from a positive to a negative angle of attack, the largest or limiting negative angle of attack possible before the membrane "pops through" is found from figure 39, where the particular excess length line crosses the 0.902 tension coefficient line. This point will correspond to the tangent point, i.e., dXL/dCT = 0 on the limiting angle of attack curve. Reducing the angle of attack further will induce the membrane to "pop through" and assume a single inverted curve shape producing negative lift. This inverted shape is similar in every respect to its positive counterpart. Experimentally the membrane "popped through" at a C_T value close to unity rather than at the theoretically predicted value of 0.902.

Figure 36 shows both a theoretical and experimental lift curve which shows good agreement and illustrates the symmetrical behavior of the membrane as it passes through the hysteresis loop.

From figure 39 it is clear that the larger the excess length the greater the spread of the hysteresis curve since larger opposite signed angles of attack are possible before pop through occurs. As mentioned earlier in this report, various degrees of flutter phenomena were observed when cross over angles of attack occurred, i.e., those angles of attack having passed through zero, which develop lift in the direction opposite to the angle of attack. Preliminary wind tunnel observation of the phenomena on the membranes used in the present tests indicate the fluttering membrane exhibits a nodal point at about the 60% chord.

Further, the intensity and frequency of the flutter is dependent on excess length, the magnitude of the angle of attack and on the tunnel dynamic pressure. Figure 40 is a mapping of the approximate regions of flutter observed with the present membranes. Stroboscopic observations of the physical system indicate that the flutter frequency band is reasonably narrow for a fixed set of conditions. However, the change of frequency with angle of attack is quite dramatic and the frequency approaches zero just before the pop through point occurs. Also the intensity of the flutter as indicated by the amplitude of the flutter and the noise generated increases rapidly soon after the system crosses the zero angle of attack. Finally it reaches a peak at an angle of attack of approximately -2° and, then, falls more slowly to zero activity as the pop through point is reached.

Previous efforts by others to construct a full scale fabric wing system for an unmanned vehicle, resulted in complex vibration problems which may be related to the flutter phenomena observed in the two-dimensional tests. Thus, a future effort might study the flutter phenomenon in the two-dimensional membrane as a introduction to the unsteady aerodynamic problems observed in previously designed three-dimensional fabric wing systems.

CONCLUSIONS

A theoretical model based on linear aerodynamics which predicts the aerodynamic behavior of two-dimensional fabric airfoils was successfully developed and validated. Wind tunnel tests were conducted on a variety of two-dimensional membrane airfoils. The data provided validation for the theoretical model. Flow visualization techniques contributed to the understanding of the physics of the flow field.

Raw two-dimensional data from the wind tunnel tests are the basis of a preliminary design data base.

The aerodynamic data collected on the two-dimensional membranes compares favorably with solid surface sectional data. For all the membranes tested a benign stall behavior was observed at all conditions tested.

This study showed that two-dimensional membranes produce lift that exceeds the lift of a flat plate by approximately 0.726 $(XL)^{\frac{1}{2}}$ within appropriate limits of angle of attack and excess length.

In all experiments for which there was excess material in the membrane positive lift was observed at negative angles of attack. Under some conditions this was accompanied by various amounts of flutter.

ACKNOWLEDGEMENTS

The author wishes to acknowledge with gratitude the invaluable assistance given to the project by Professor H. C. Curtiss, Jr. and Brooke Smith of the Mechanical and Aerospace Engineering Department of Princeton University.

REFERENCES

1. Kuethe, A. M. and Chow, C.-Y., "Foundations of Aerodynamics", John Wiley and Sons, 1976.

2. Timoshenko, S. and Woinowsky-Kreiger, S., "Theory of Plates and Shells", McGraw-Hill, 1959.

3. Thwaites, B. "The Aerodynamic Theory of Sails, I, Two-Dimensional Sails", Proceedings of the Royal Society, Series A, No. 1306, Vol. 261, 16 May 1961.

4. Nielsen, J. N. "Theory of Flexible Aerodynamic Surfaces", Journal of Applied Mechanics, September 1963.

5. James, R. M. "On the Remarkable Accuracy of the Vortex Lattice Method", Computer Methods in Applied Mechanics and Engineering I (1972) p. 59-79.

TABLE I

DEFINITION OF MATRICES

[C] Matrix with p + 1 columns, p rows, $[C] = \begin{bmatrix} 1 & 1 & 0 & 0 & \cdots & \\ 0 & 1 & 1 & 0 & 0 \cdots & \\ 0 & 0 & 1 & 1 & 0 \cdots & \\ \vdots & & & & & \\ 0 & 0 & 0 & 0 & 0 \cdots & 1 \quad 1 \end{bmatrix}$

[E] Matrix with p + 1 columns, p rows, $[E] = \begin{bmatrix} 1 & -1 & 0 & 0 & \cdots & \\ 0 & 1 & -1 & 0 & \cdots & \\ 0 & 0 & 1 & -1 & 0 \cdots & \\ \vdots & & & & & \\ 0 & 0 & 0 & 0 & 0 \cdots & 1 \quad -1 \end{bmatrix}$

[G*] p x p matrix, $[G^*] = \begin{bmatrix} 1 & 1 & 0 & 0 \cdots \cdots \\ 0 & 1 & 1 & 0 \cdots \cdots \\ 0 & 0 & 1 & 1 \cdots \cdots \\ \vdots & & & \\ 0 & 0 & 0 & 0 \quad 0 \cdots \quad 0 \end{bmatrix}$

[H*] p x p matrix, $[H^*] = \begin{bmatrix} 1 & -1 & 0 & 0 & 0 \cdots \\ 0 & 1 & -1 & 0 & 0 \cdots \\ 0 & 0 & 1 & -1 & 0 \cdots \\ \vdots & & & & \\ 1 & 1 & 1 & 1 & 1 \cdots \quad 1 \end{bmatrix}$

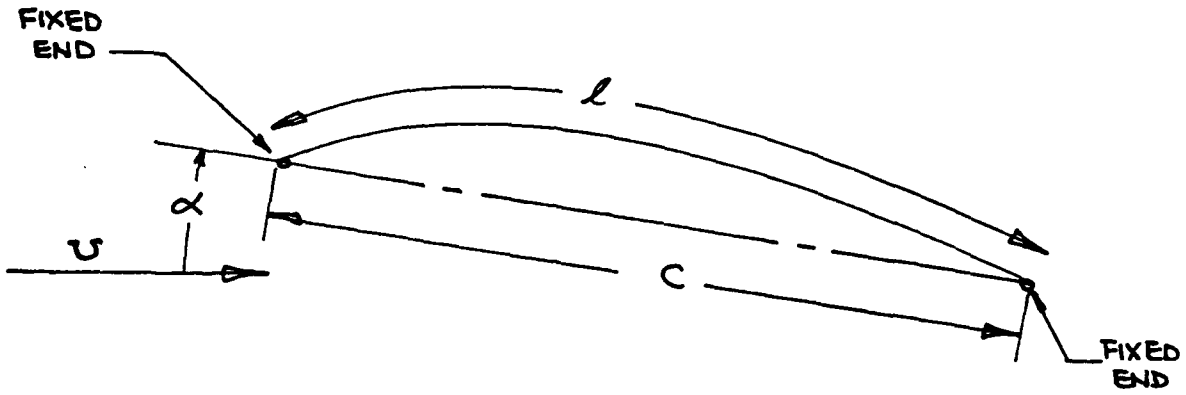

ℓ, C SPECIFIED, TENSION IN MEMBRANE UNKNOWN
SHAPE UNKNOWN

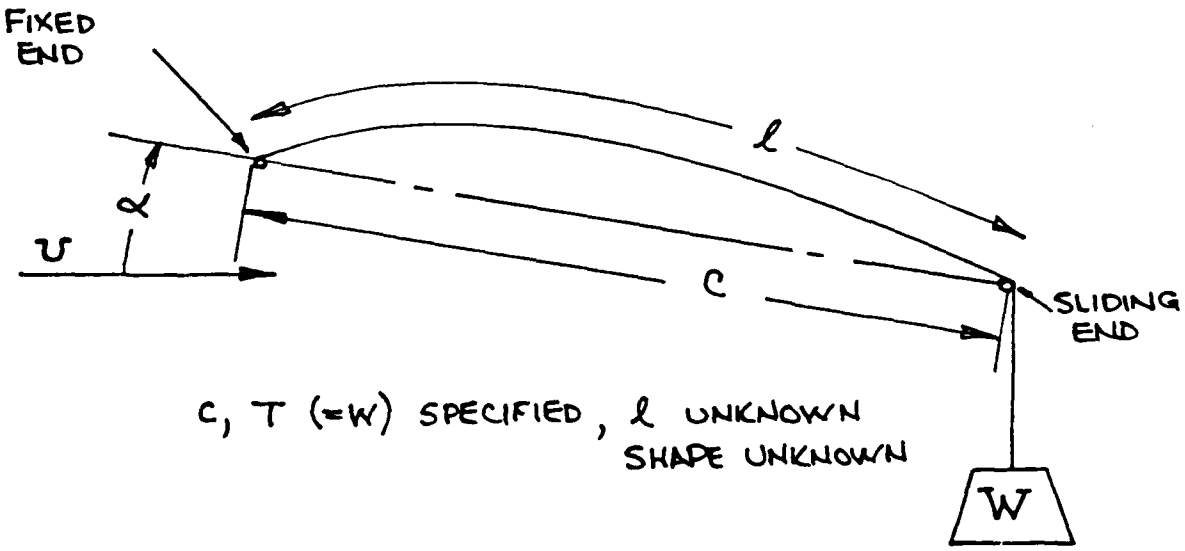

C, T (=W) SPECIFIED, ℓ UNKNOWN
SHAPE UNKNOWN

Figure 1. Two Approaches to Membrane Airfoil Theory

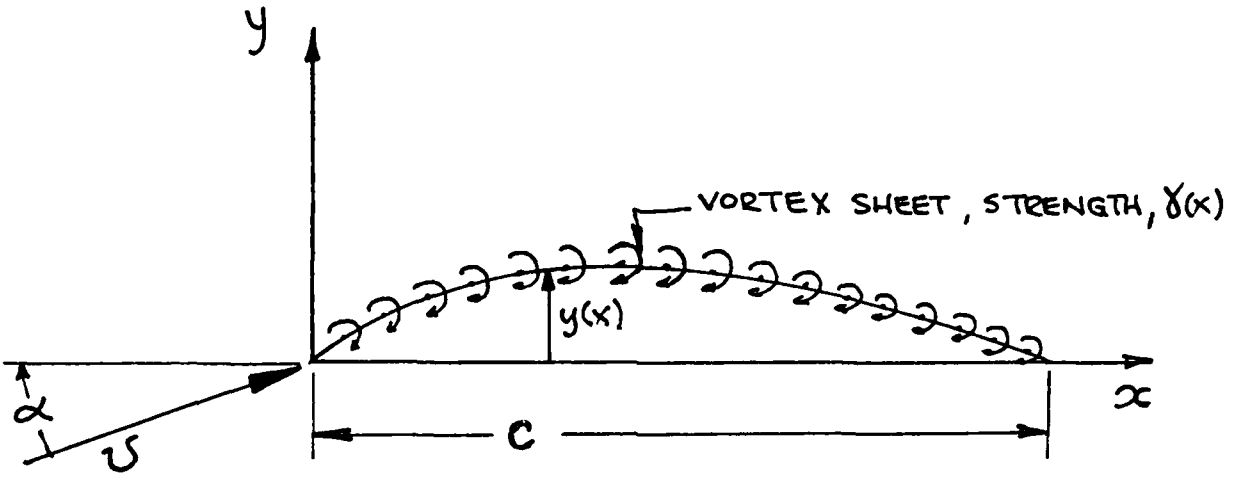

Figure 2. Geometry and Coordinate System for Aerodynamic Relationships

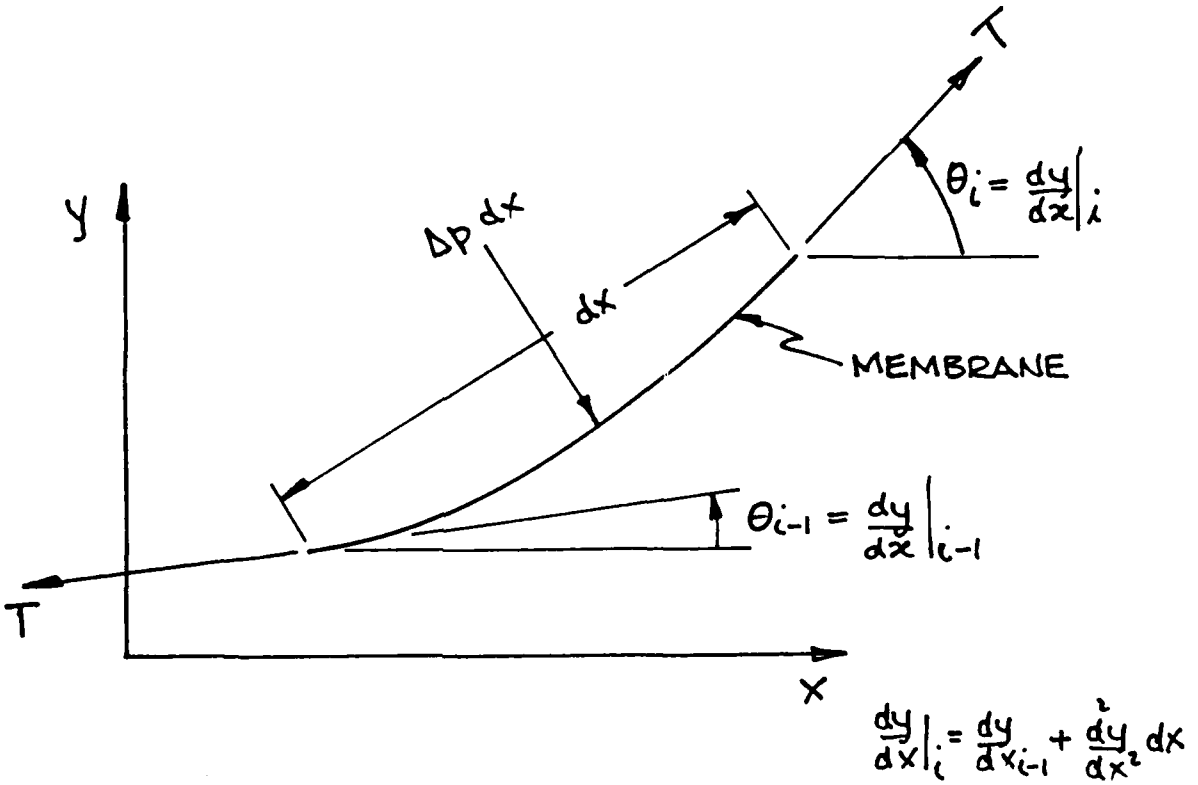

Figure 3. Geometry and Relationships for Force Balance on Membrane

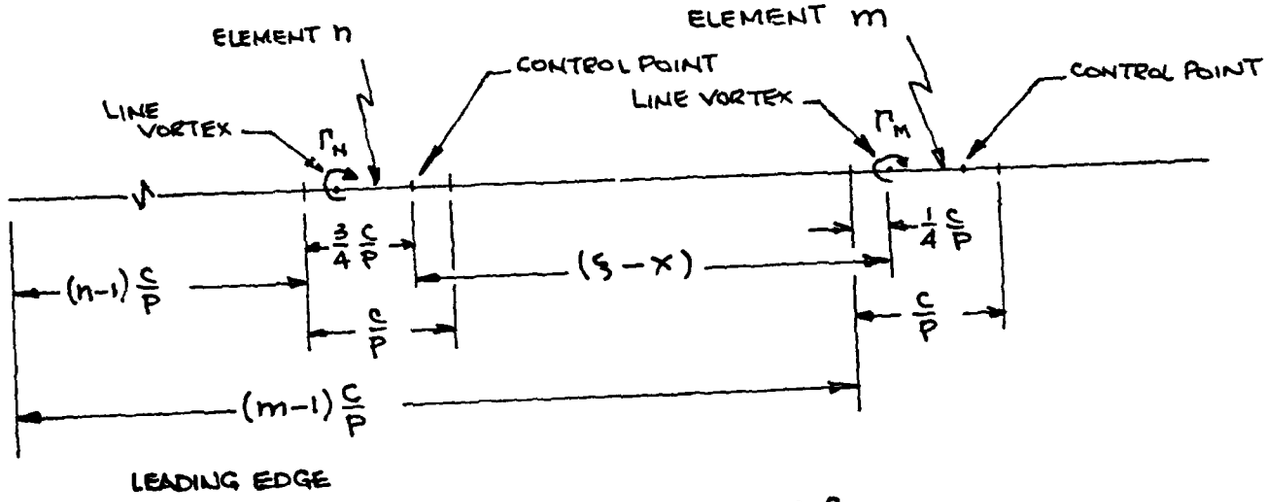

$$(\xi - x) = (m - n - \tfrac{1}{2})\frac{c}{p}$$

Figure 4. Geometry for Vortex Lattice Representation of Airfoil

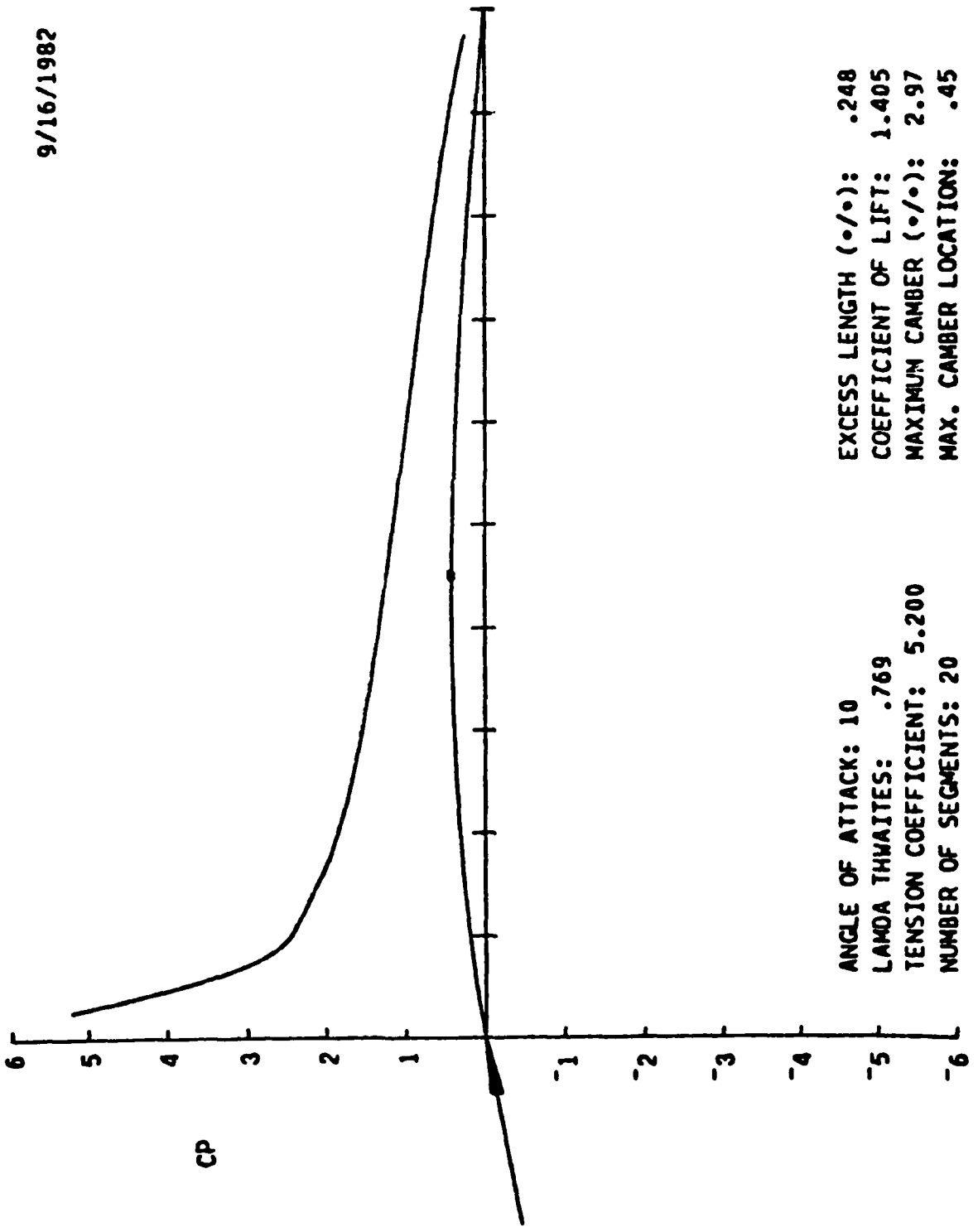

Figure 5. Theoretical Membrane Shape and Pressure Distribution

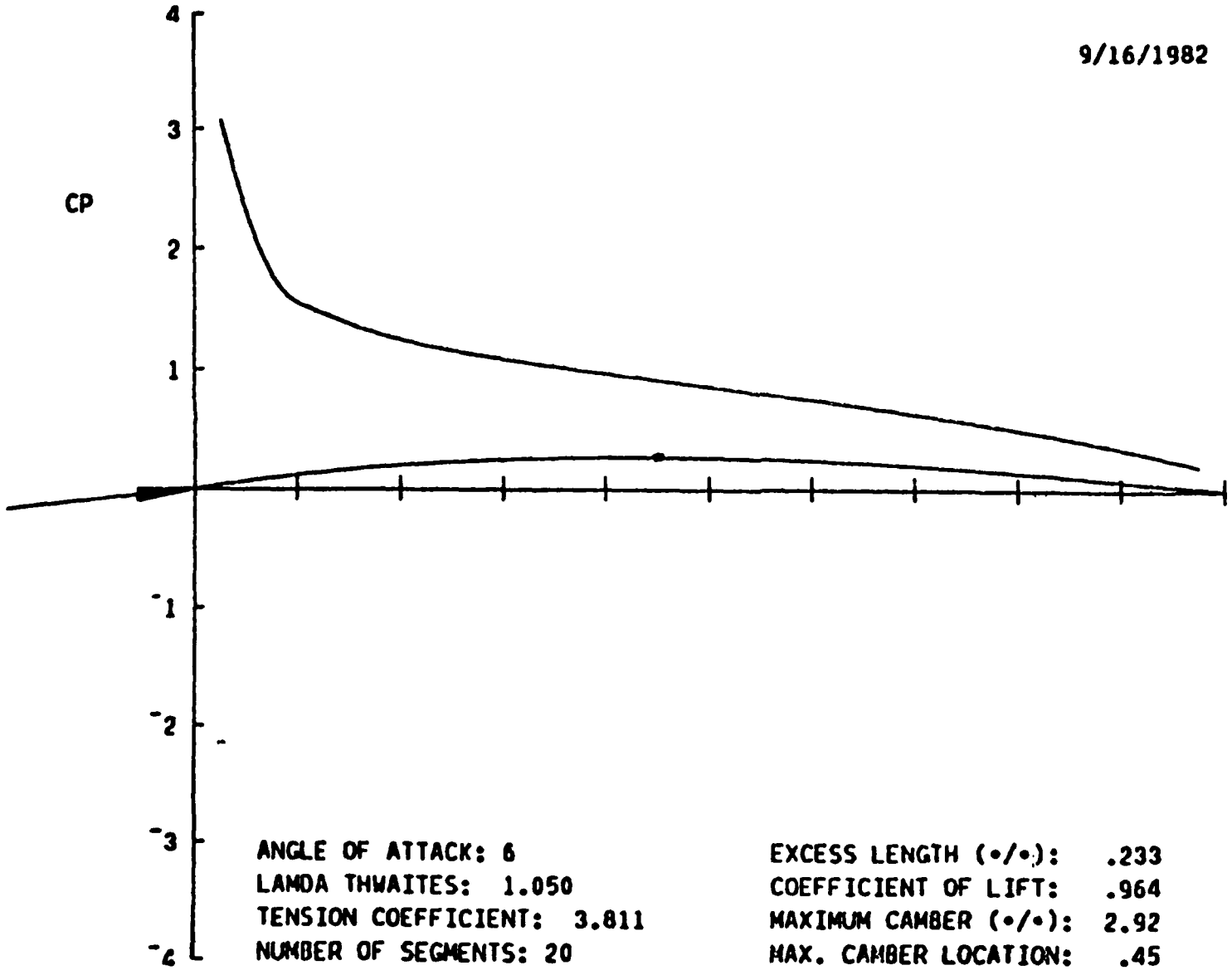

Figure 6. Theoretical Membrane Shape and Pressure Distribution

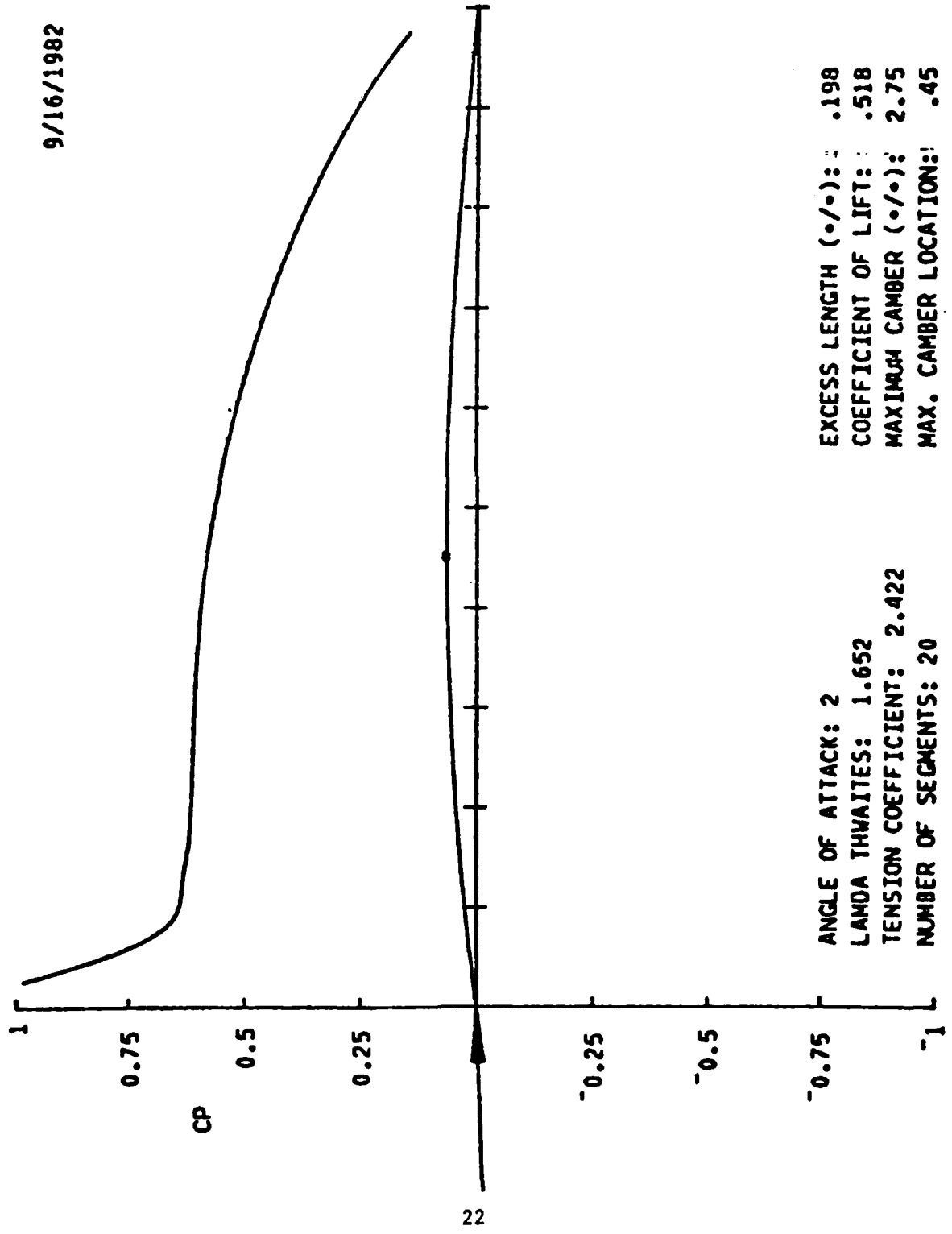

Figure 7. Theoretical Membrane Shape and Pressure Distribution

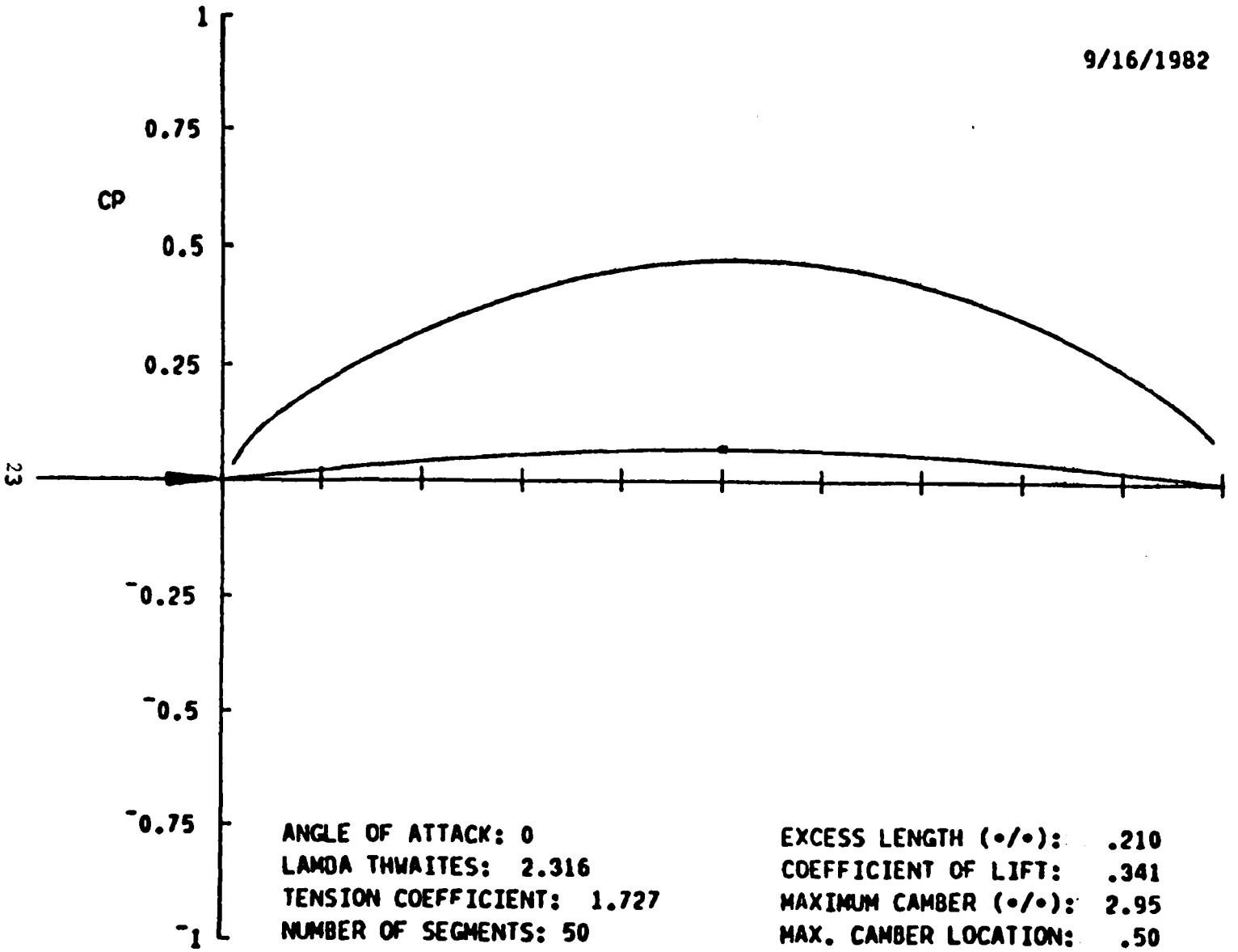

NADC-83096-60

Figure 8. Theoretical Membrane Shape and Pressure Distribution

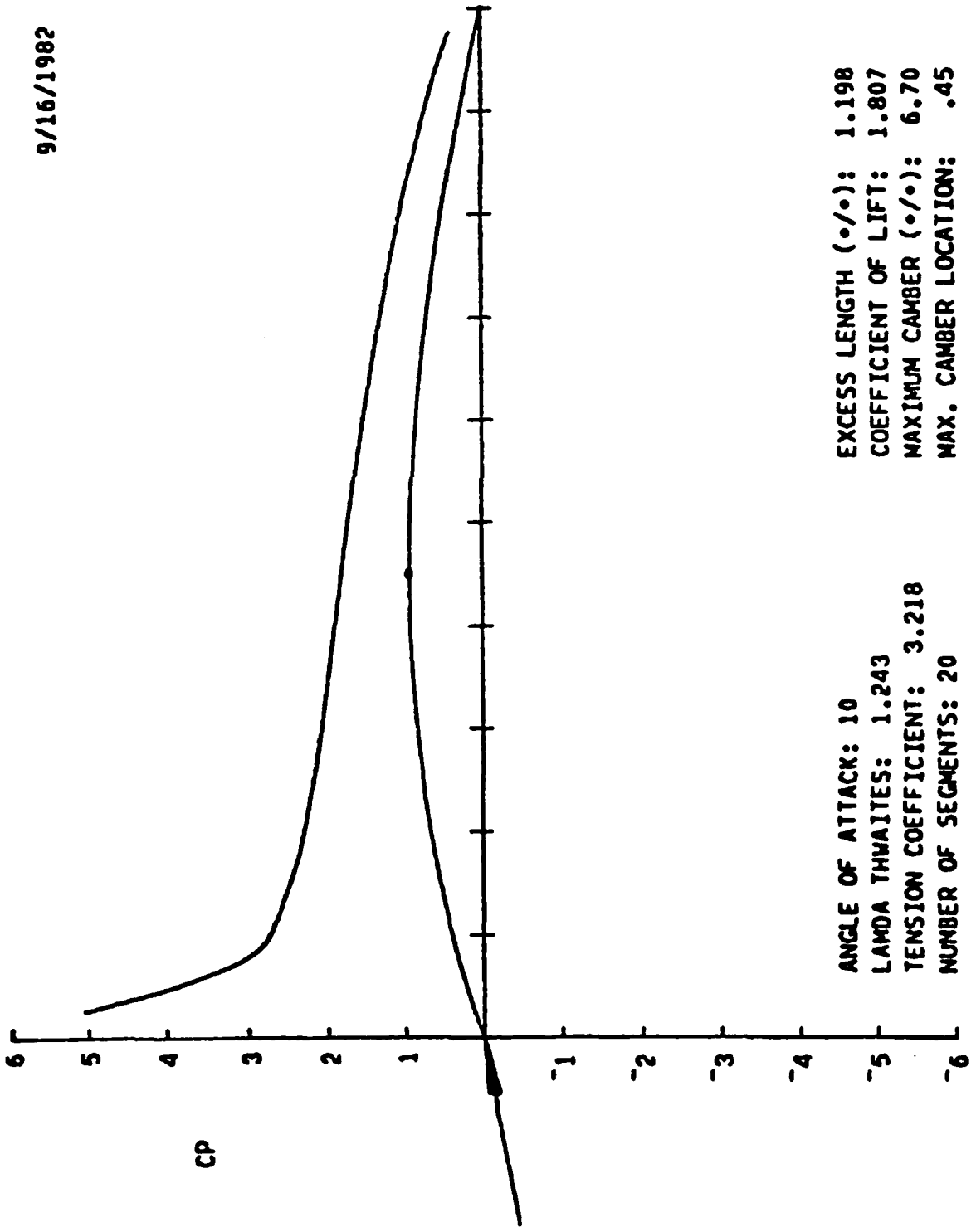

Figure 9. Theoretical Membrane Shape and Pressure Distribution

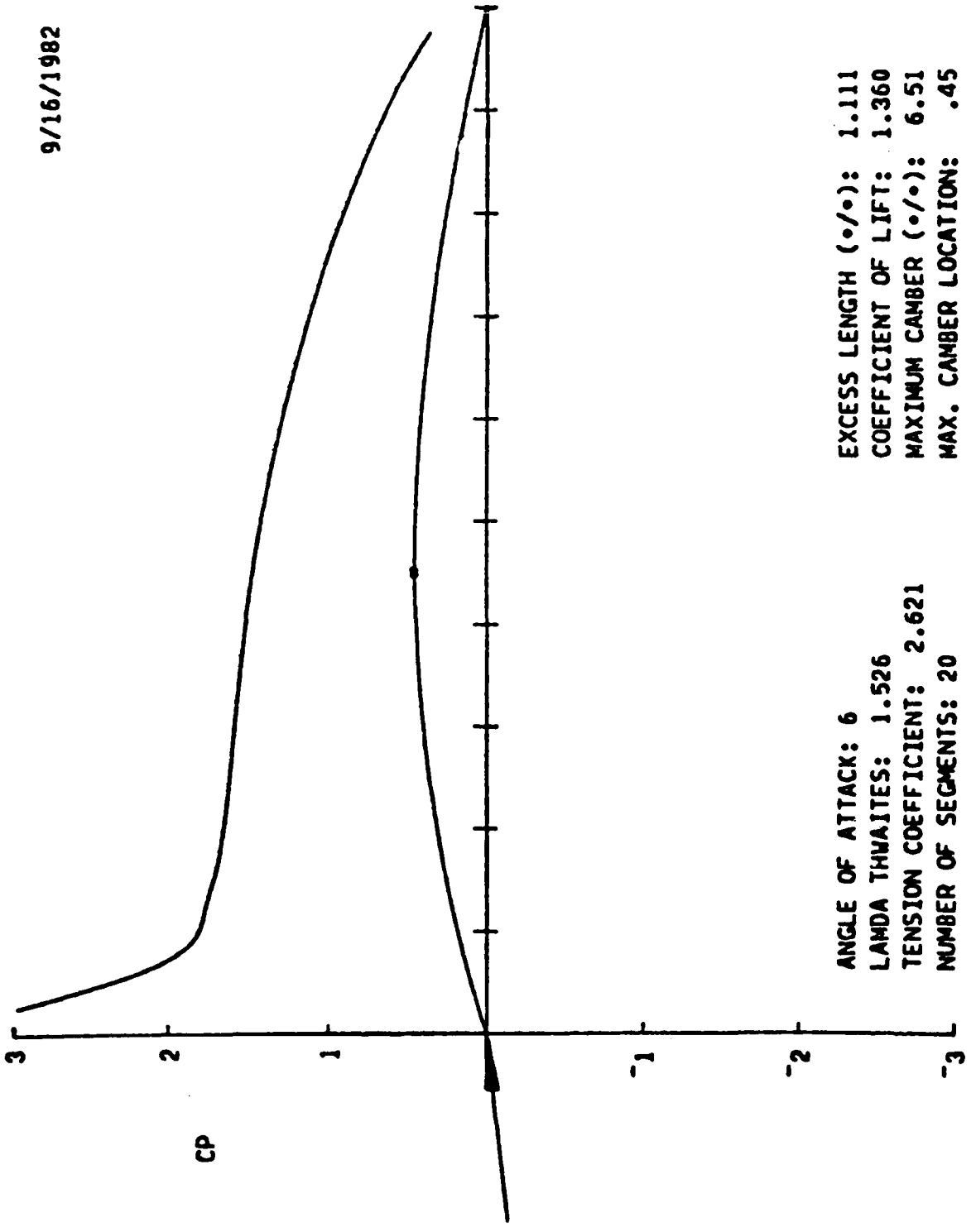

Figure 10. Theoretical Membrane Shape and Pressure Distribution

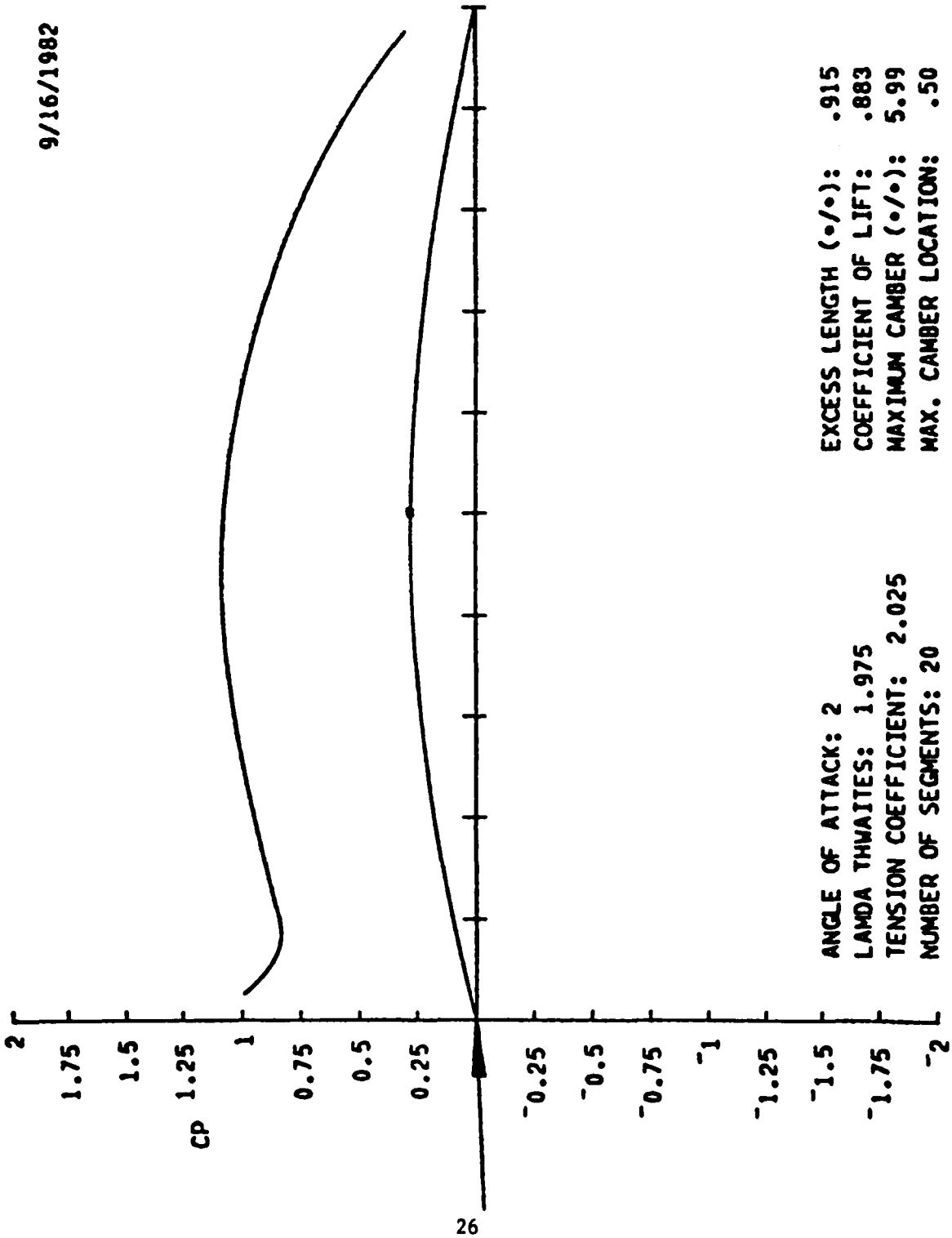

Figure 11. Theoretical Membrane Shape and Pressure Distribution

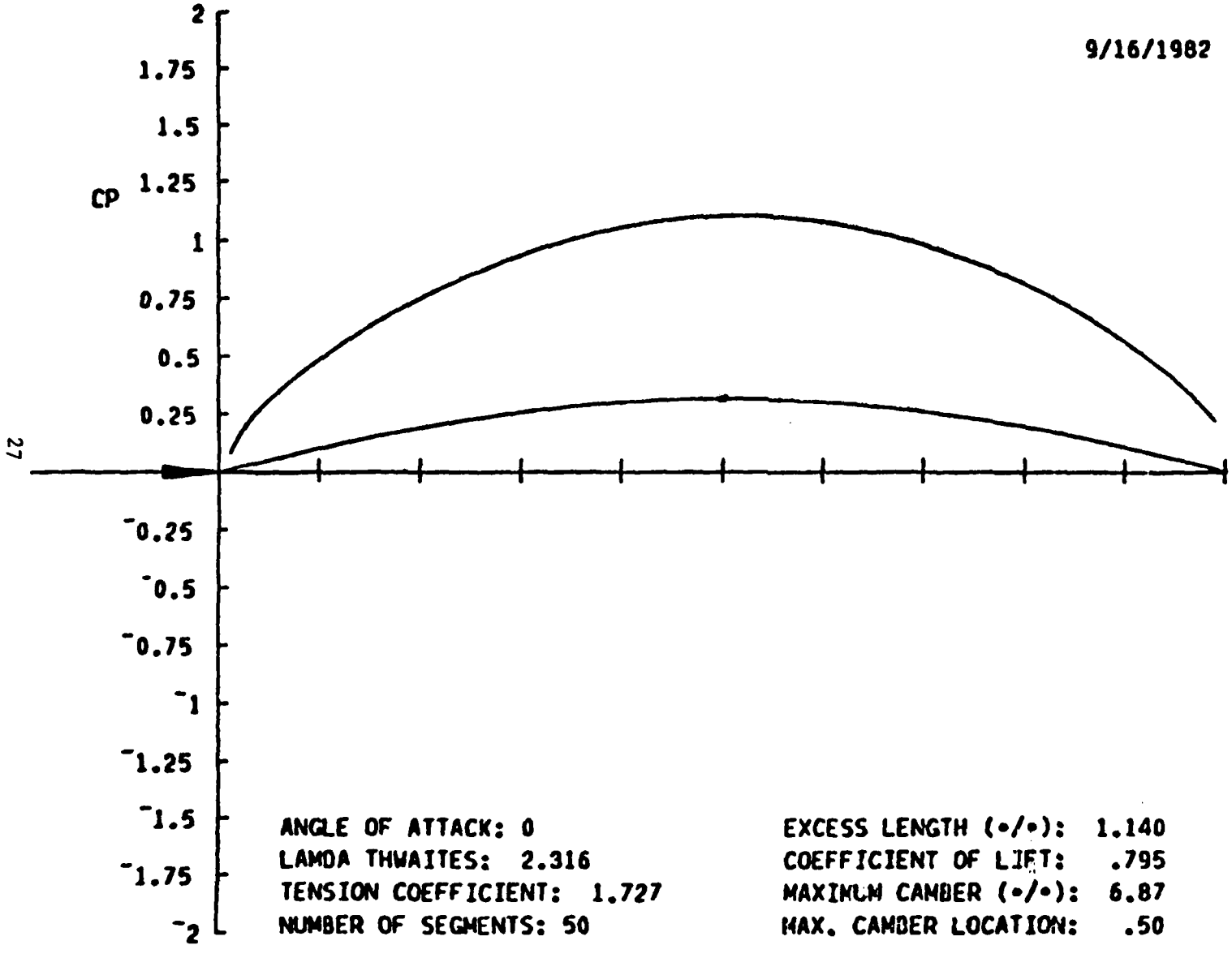

Figure 12. Theoretical Membrane Shape and Pressure Distribution

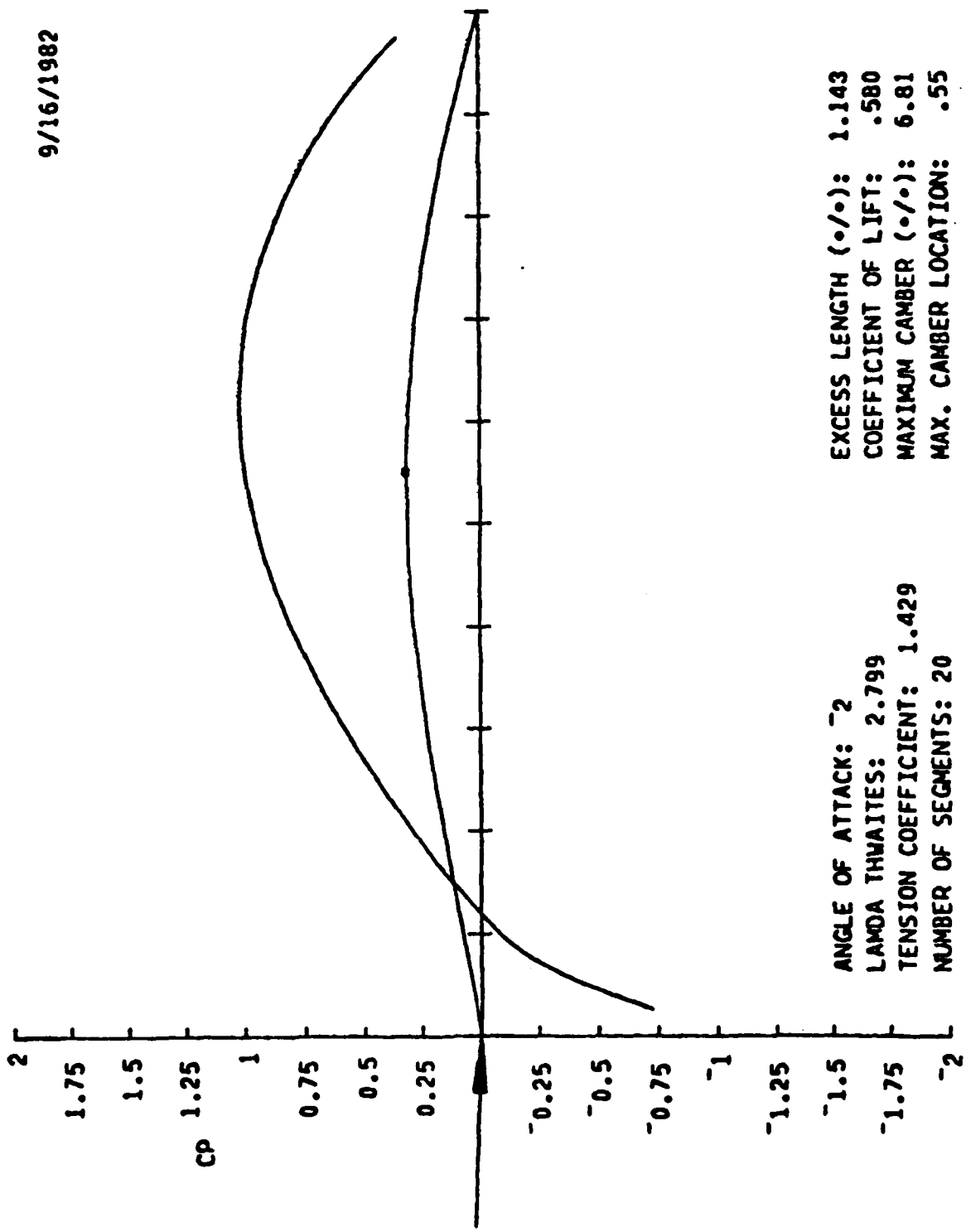

Figure 13. Theoretical Membrane Shape and Pressure Distribution

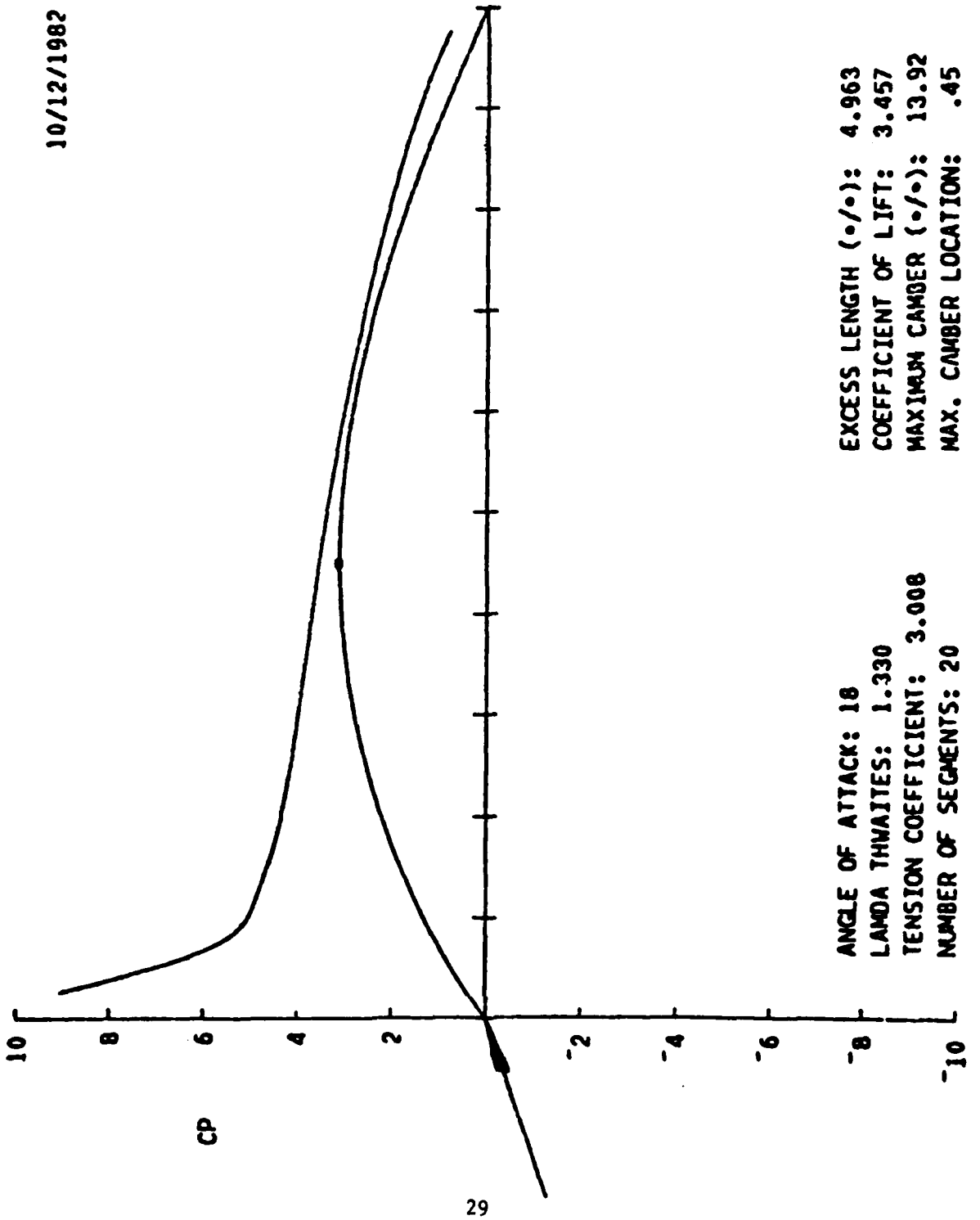
10/12/1982
CP
10
8
6
4
2
-2
-4
-6
-8
-10
ANGLE OF ATTACK: 18
LAMDA THWAITES: 1.330
TENSION COEFFICIENT: 3.008
NUMBER OF SEGMENTS: 20
EXCESS LENGTH (•/•): 4.963
COEFFICIENT OF LIFT: 3.457
MAXIMUM CAMBER (•/•): 13.92
MAX. CAMBER LOCATION: .45

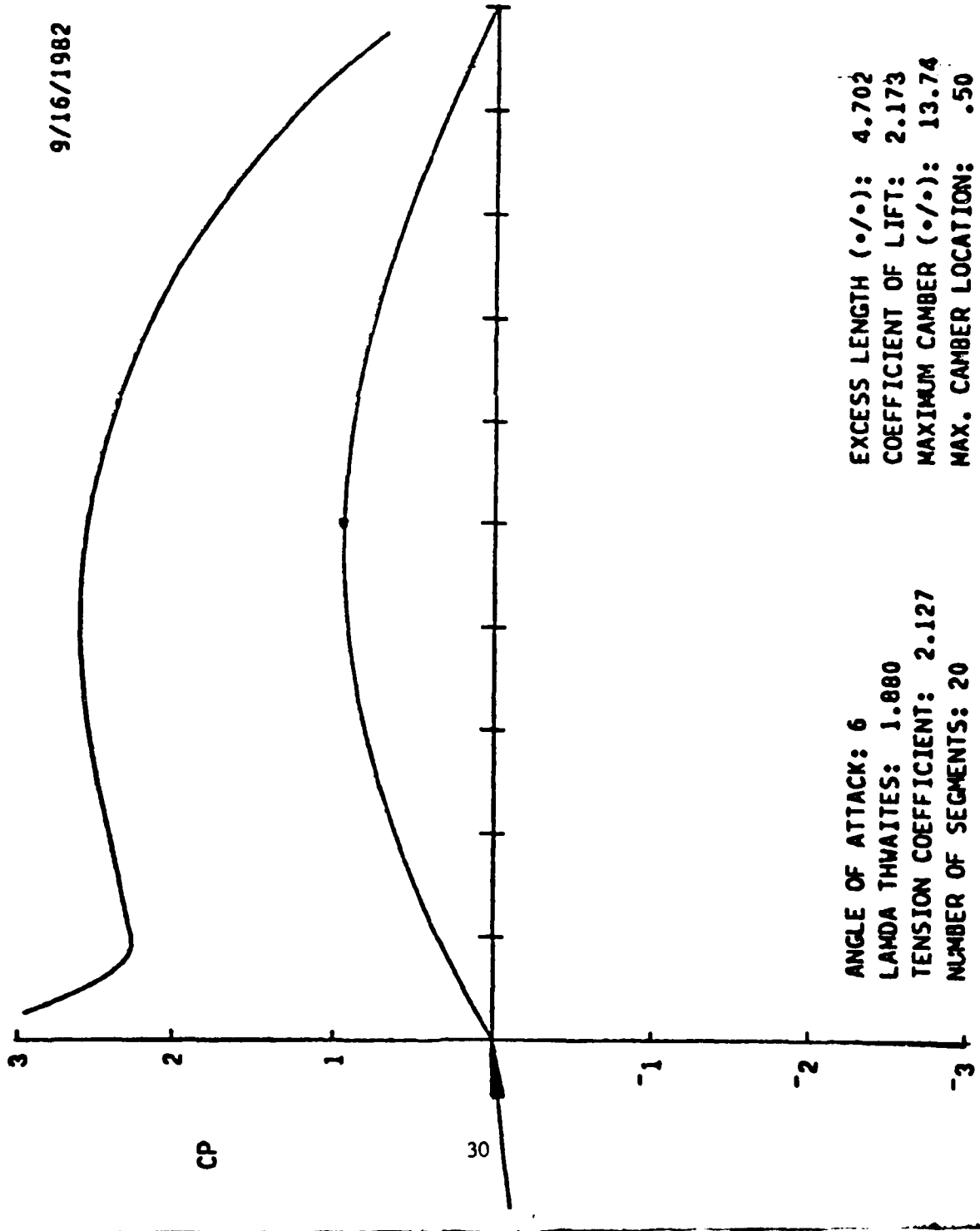

Figure 15. Theoretical Membrane Shape and Pressure Distribution

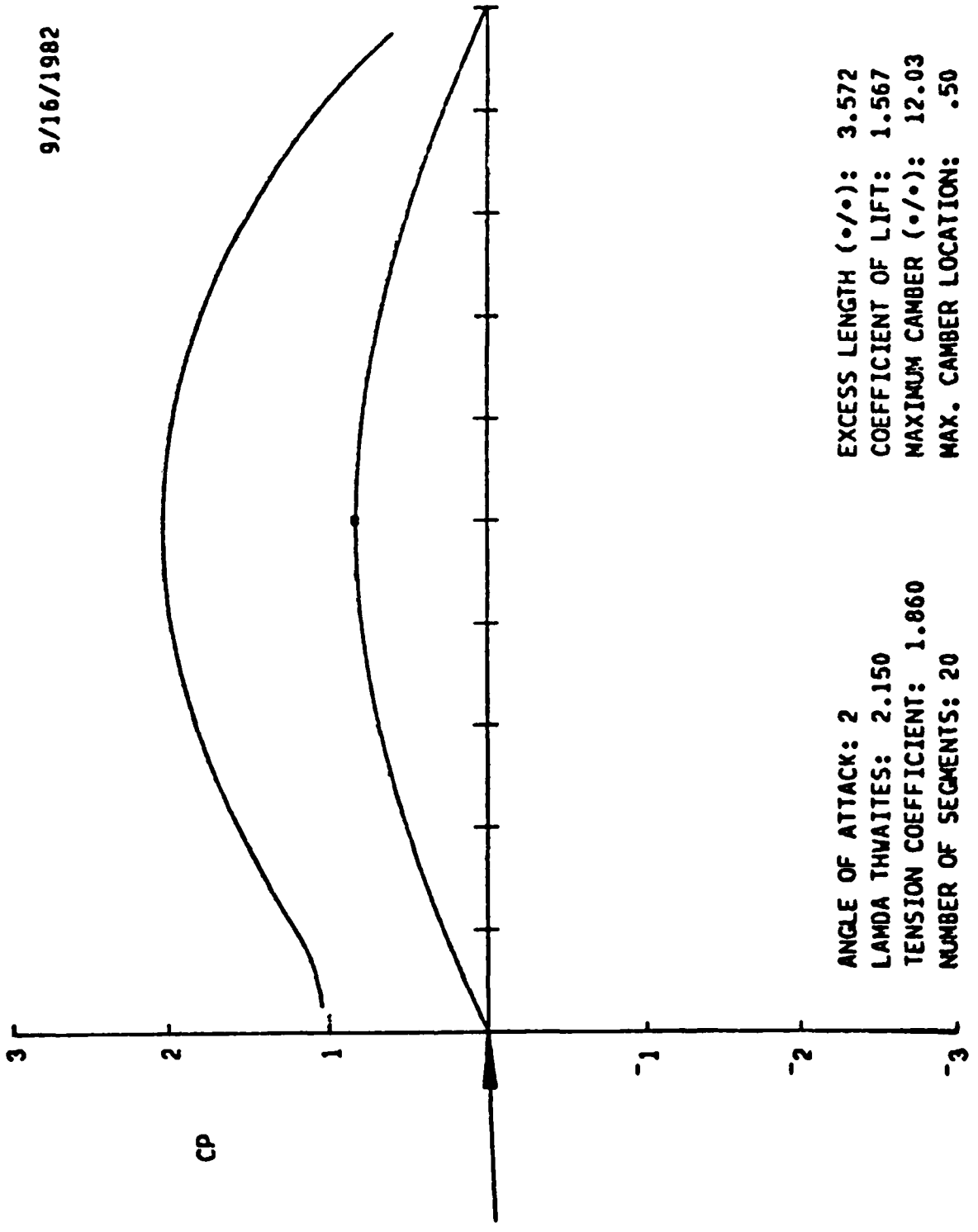

Figure 16. Theoretical Membrane Shape and Pressure Distribution

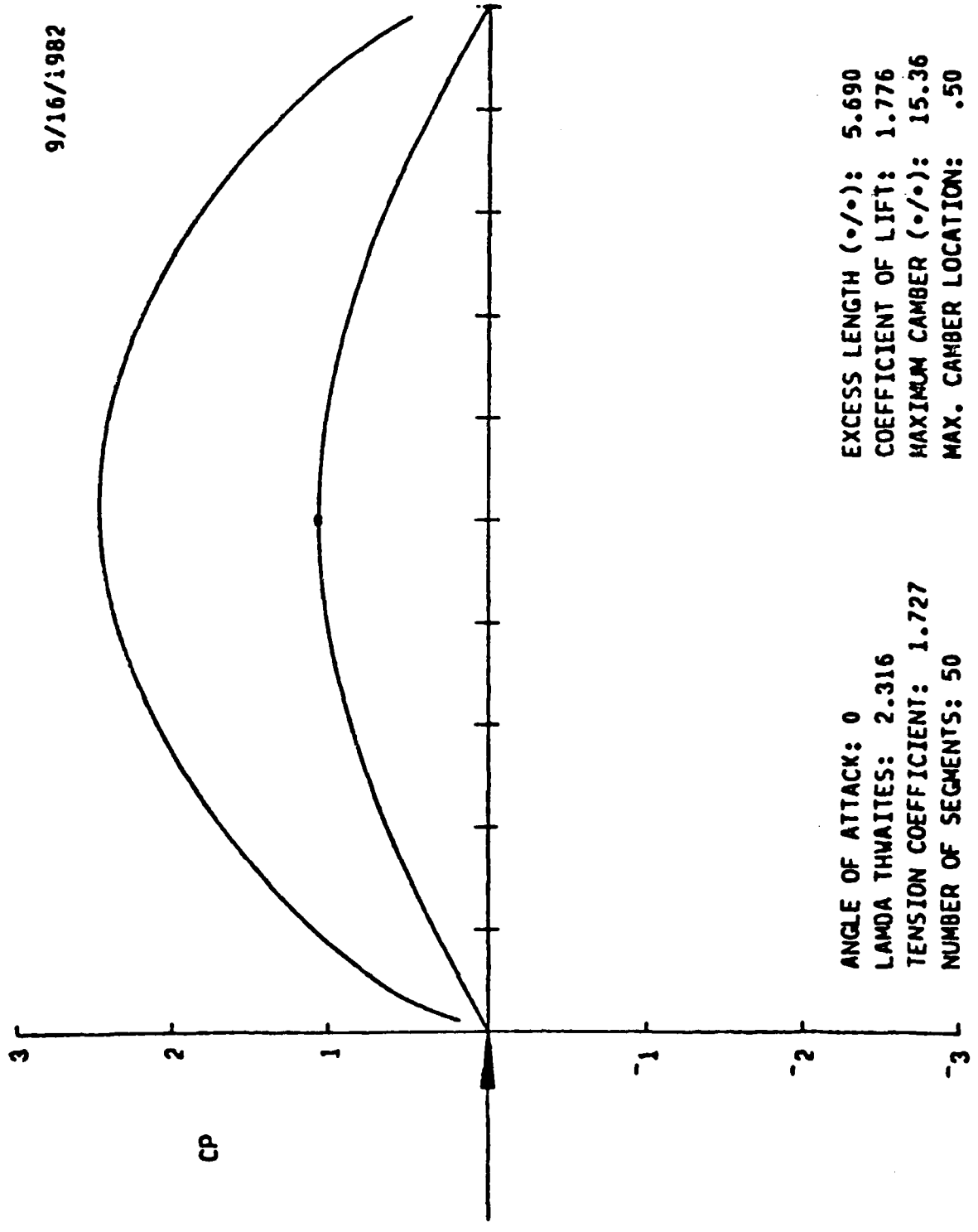

Figure 17. Theoretical Membrane Shape and Pressure Distribution

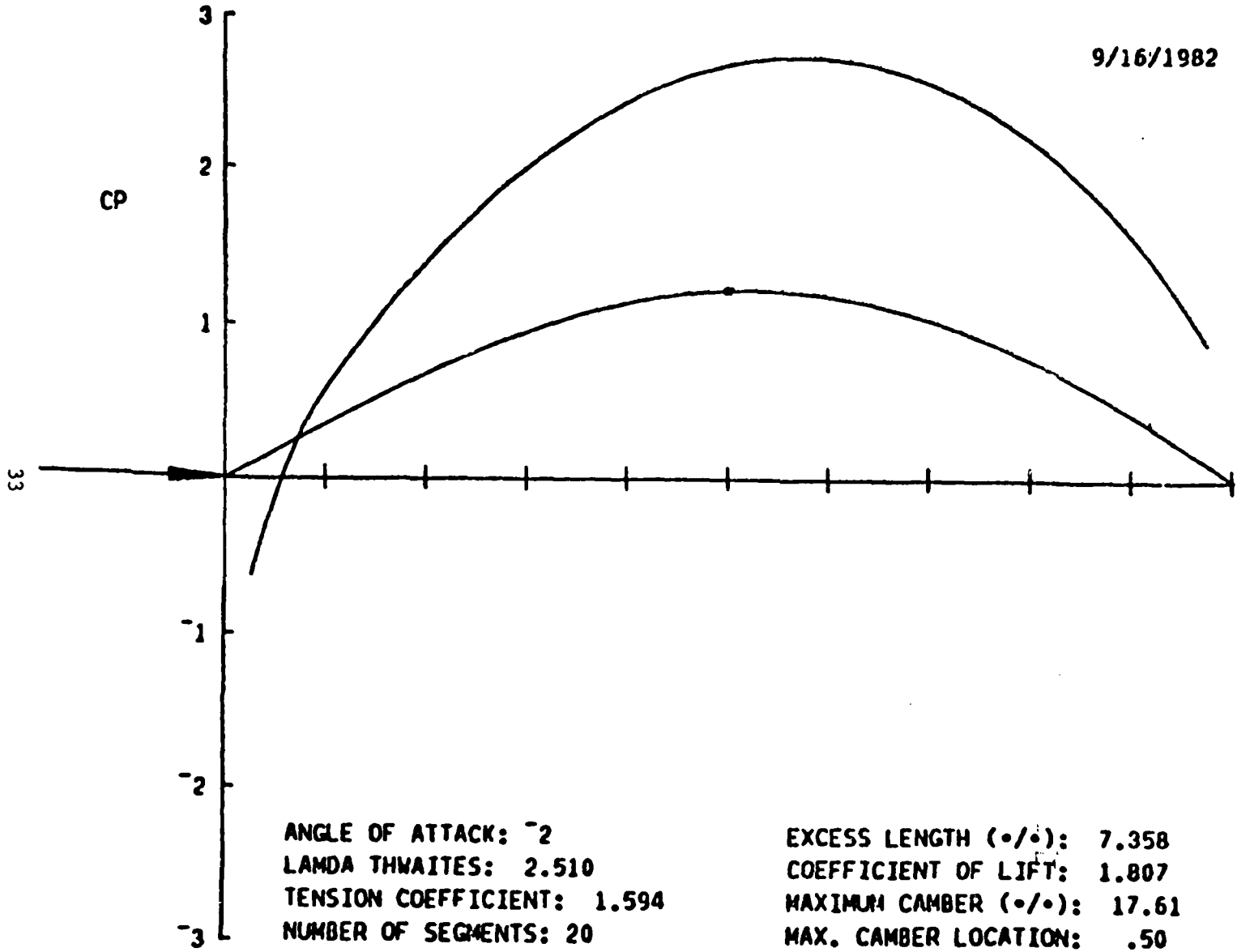

Figure 18. Theoretical Membrane Shape and Pressure Distribution

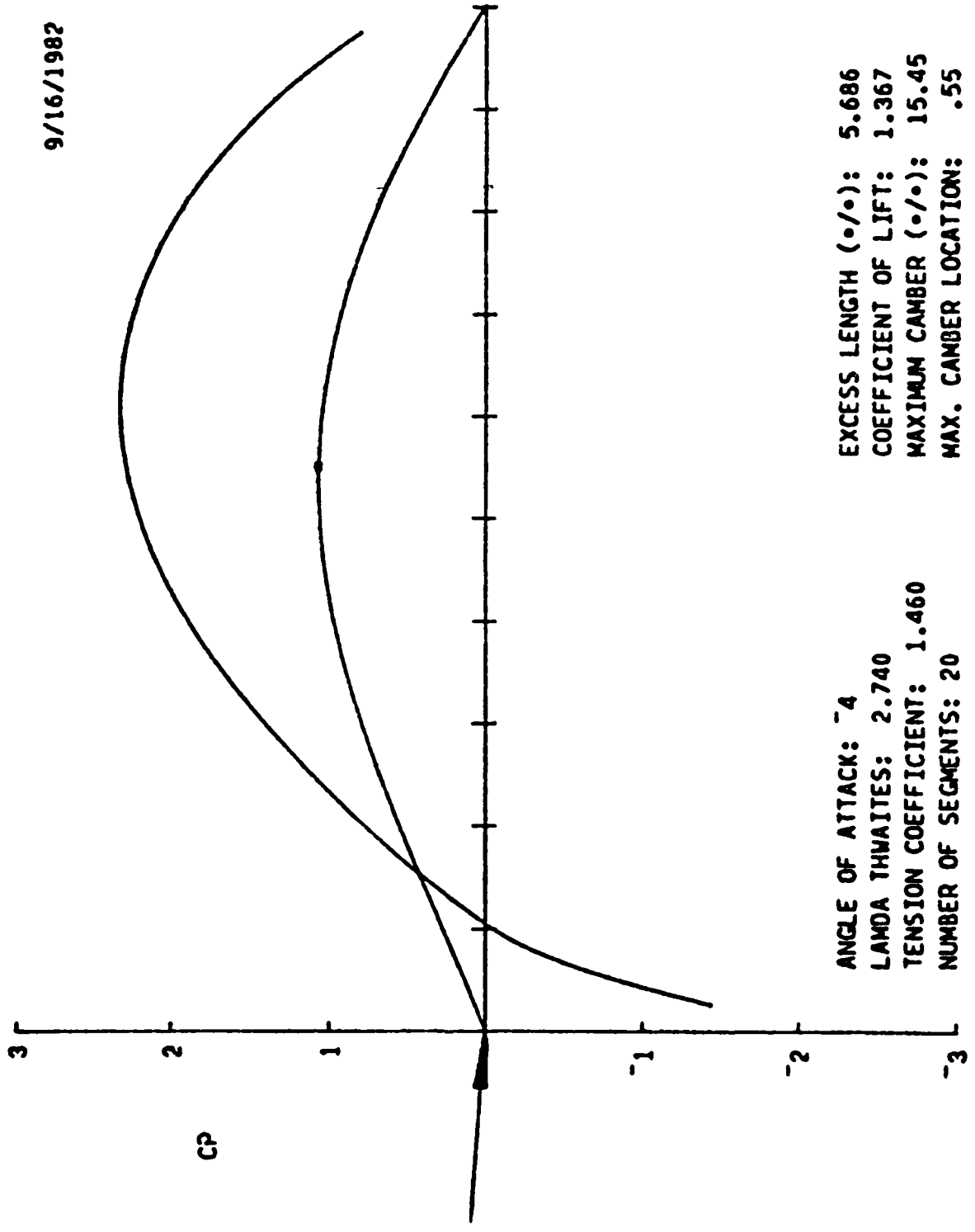

Figure 19. Theoretical Membrane Shape and Pressure Distribution

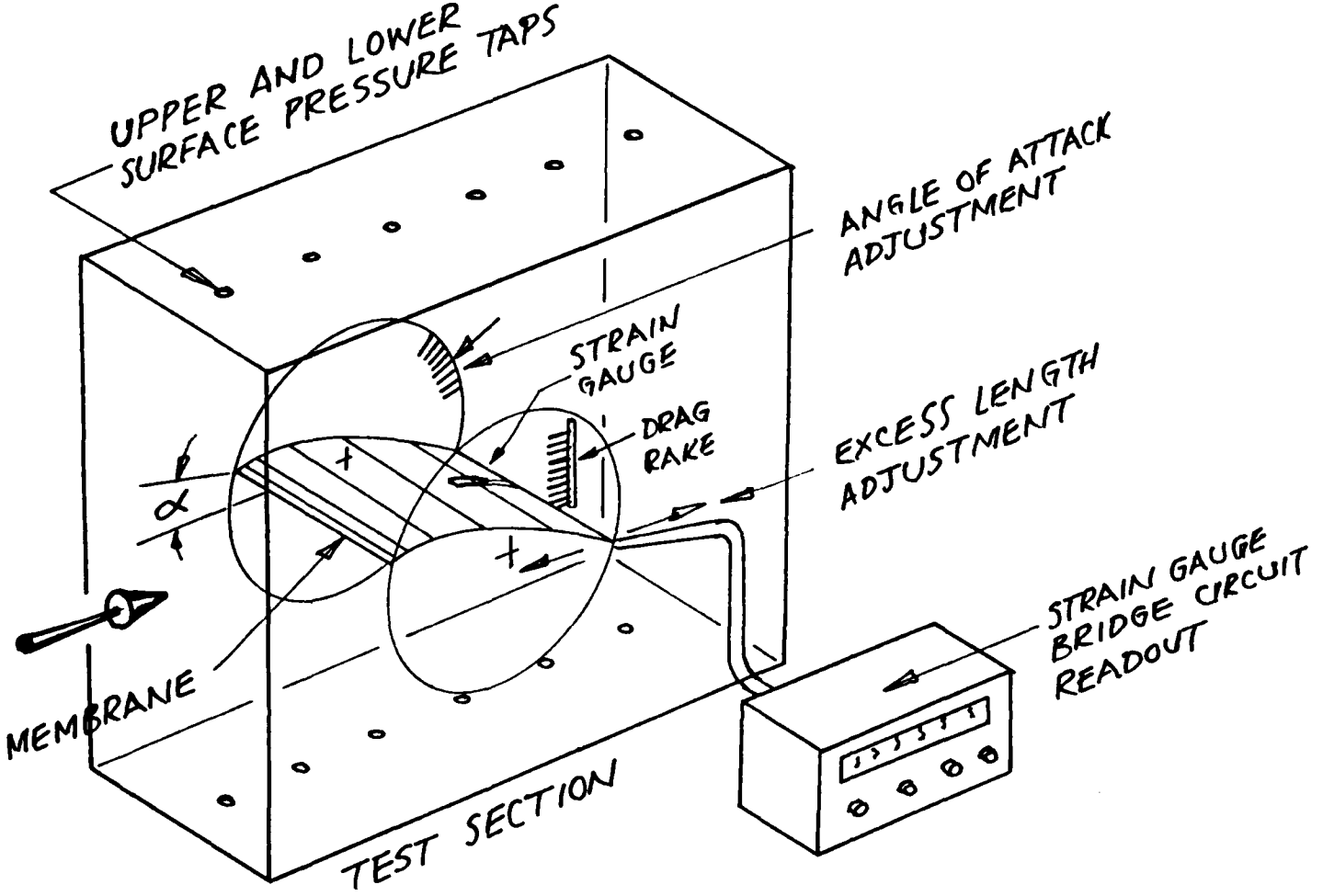

Figure 20. Wind Tunnel Test Section

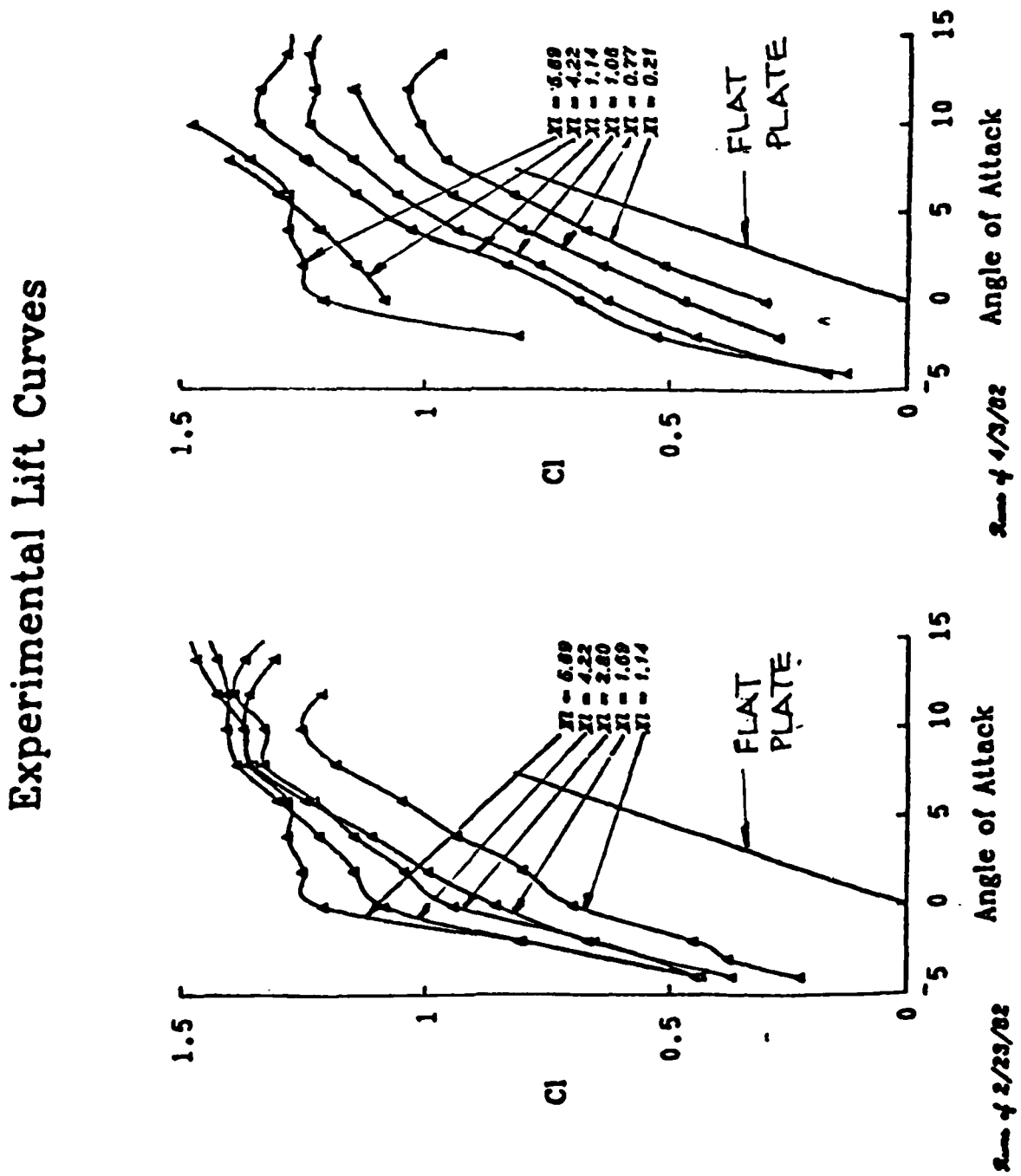

Figure 21. Experimental Lift Curves

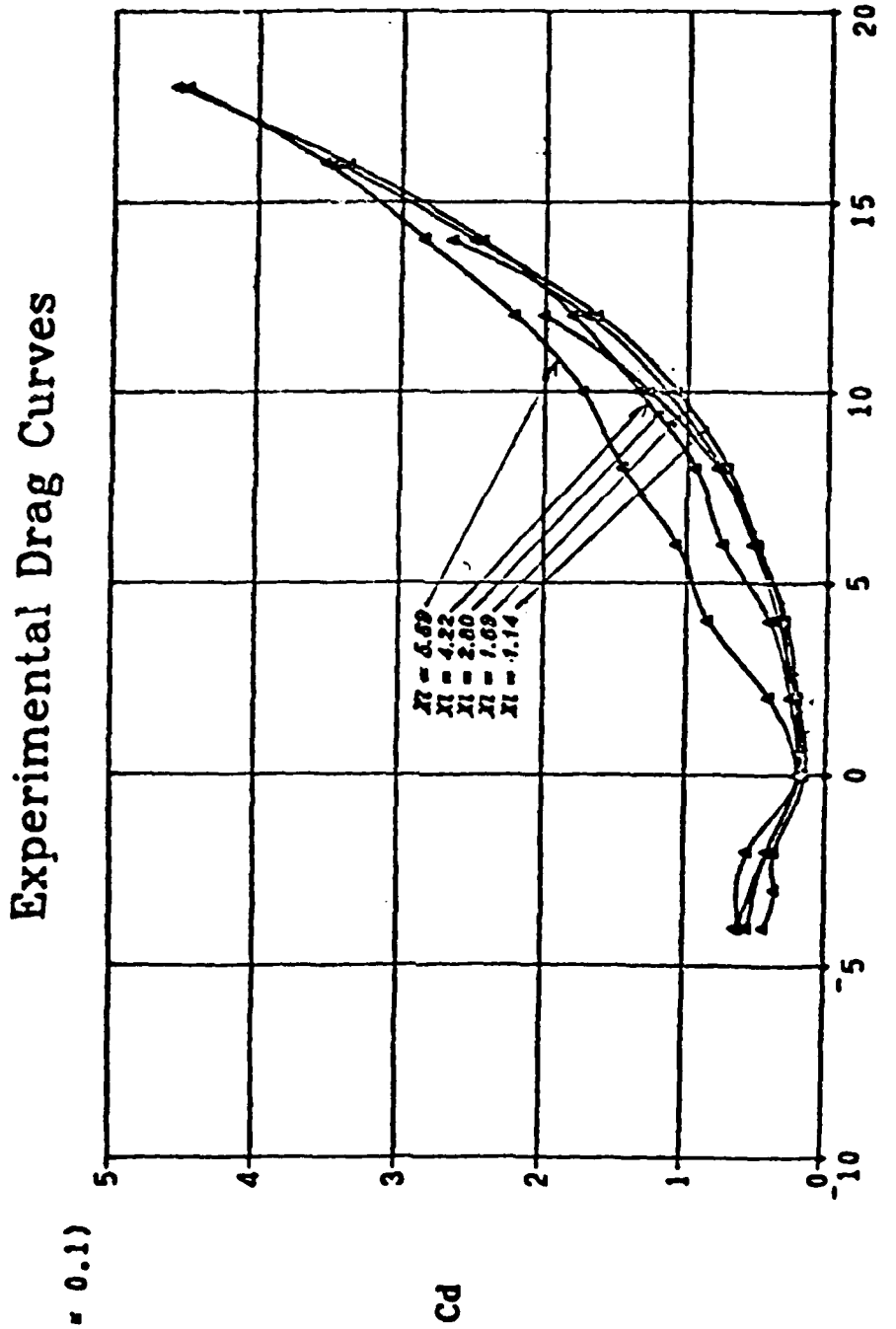

Figure 22. Experimental Drag Curves

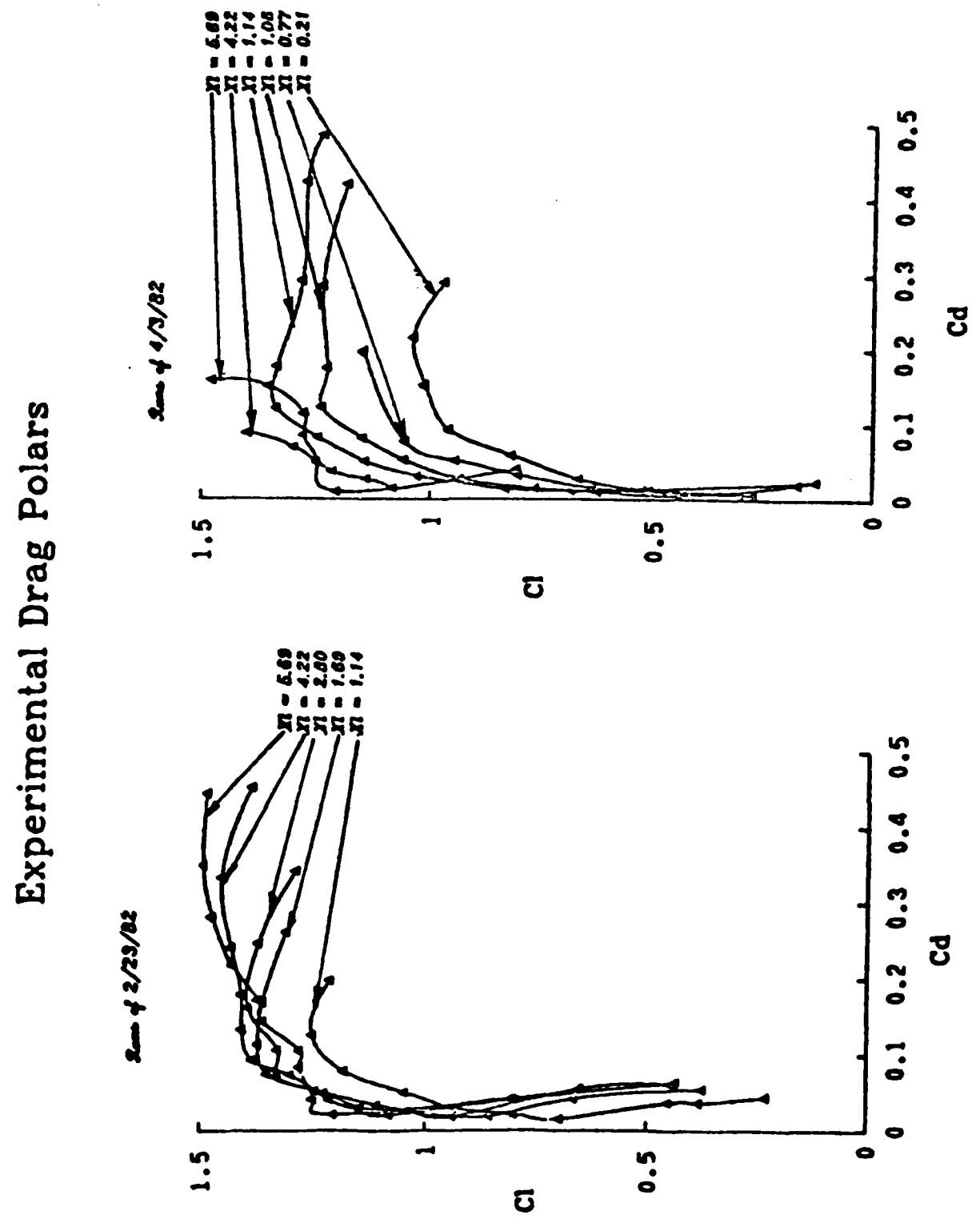

Figure 23. Experimental Drag Polars

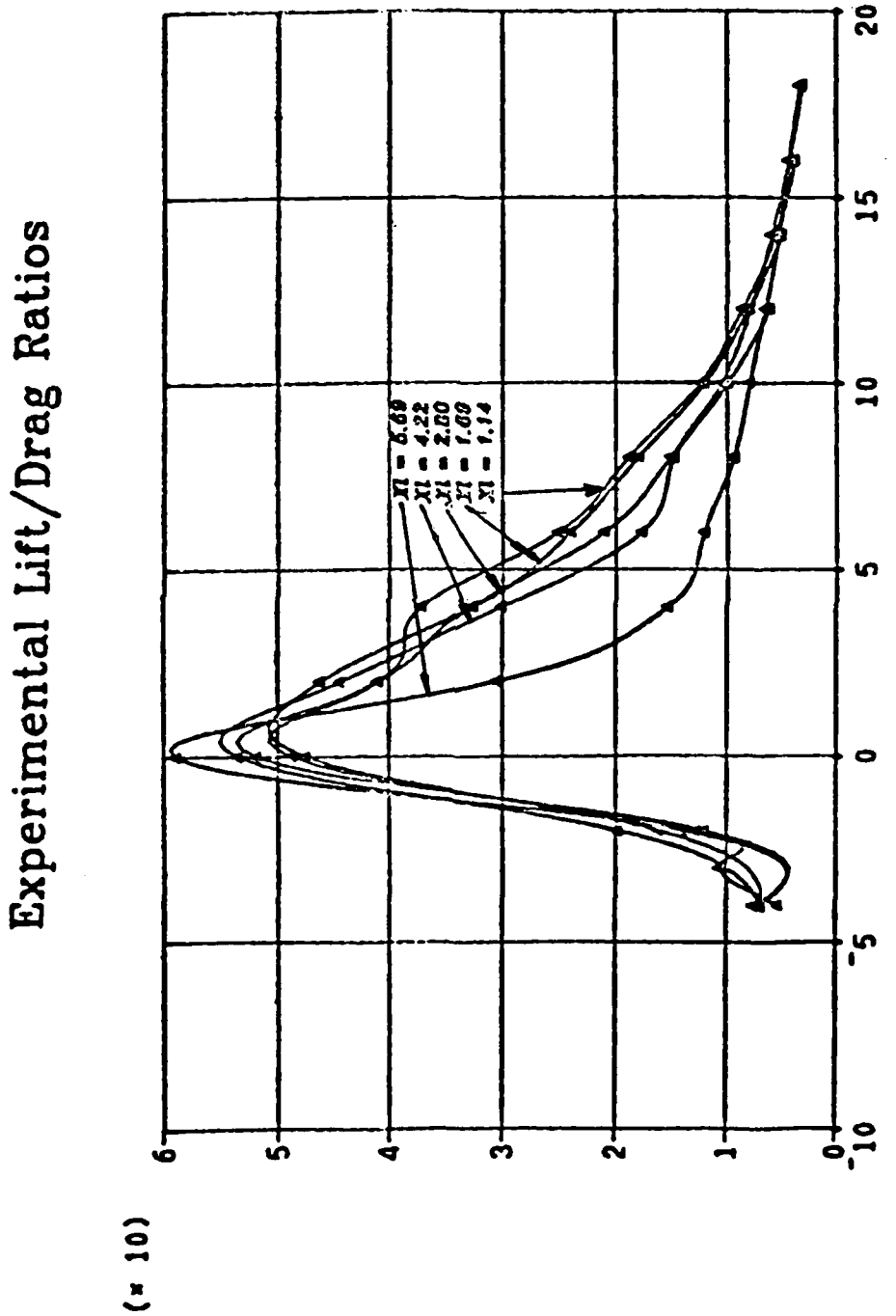

Figure 24. Experimental Lift to Drag Ratios

Lift Curves

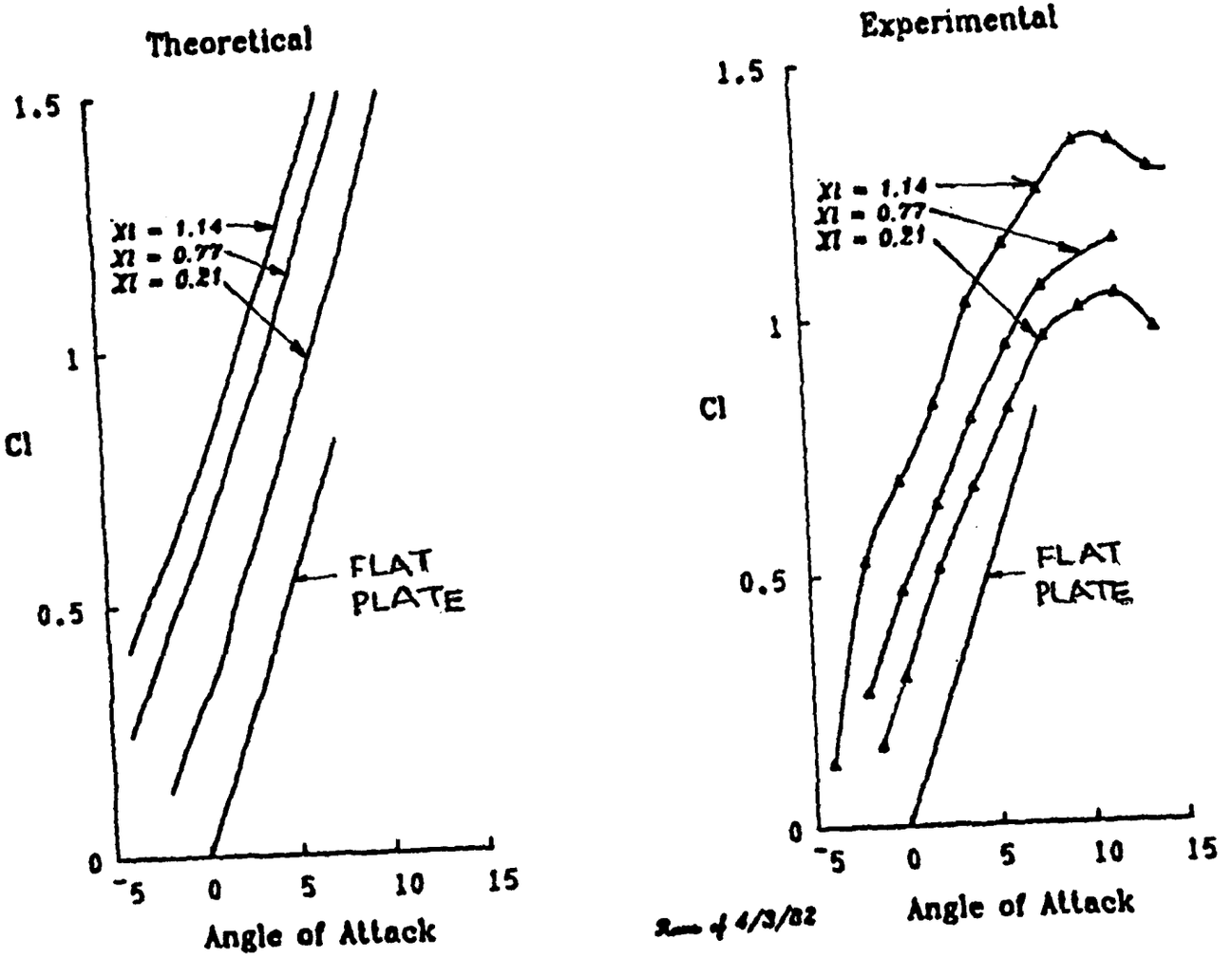

Figure 25. A Comparison of Theoretical and Experimental Lift Curves

Tension Curves

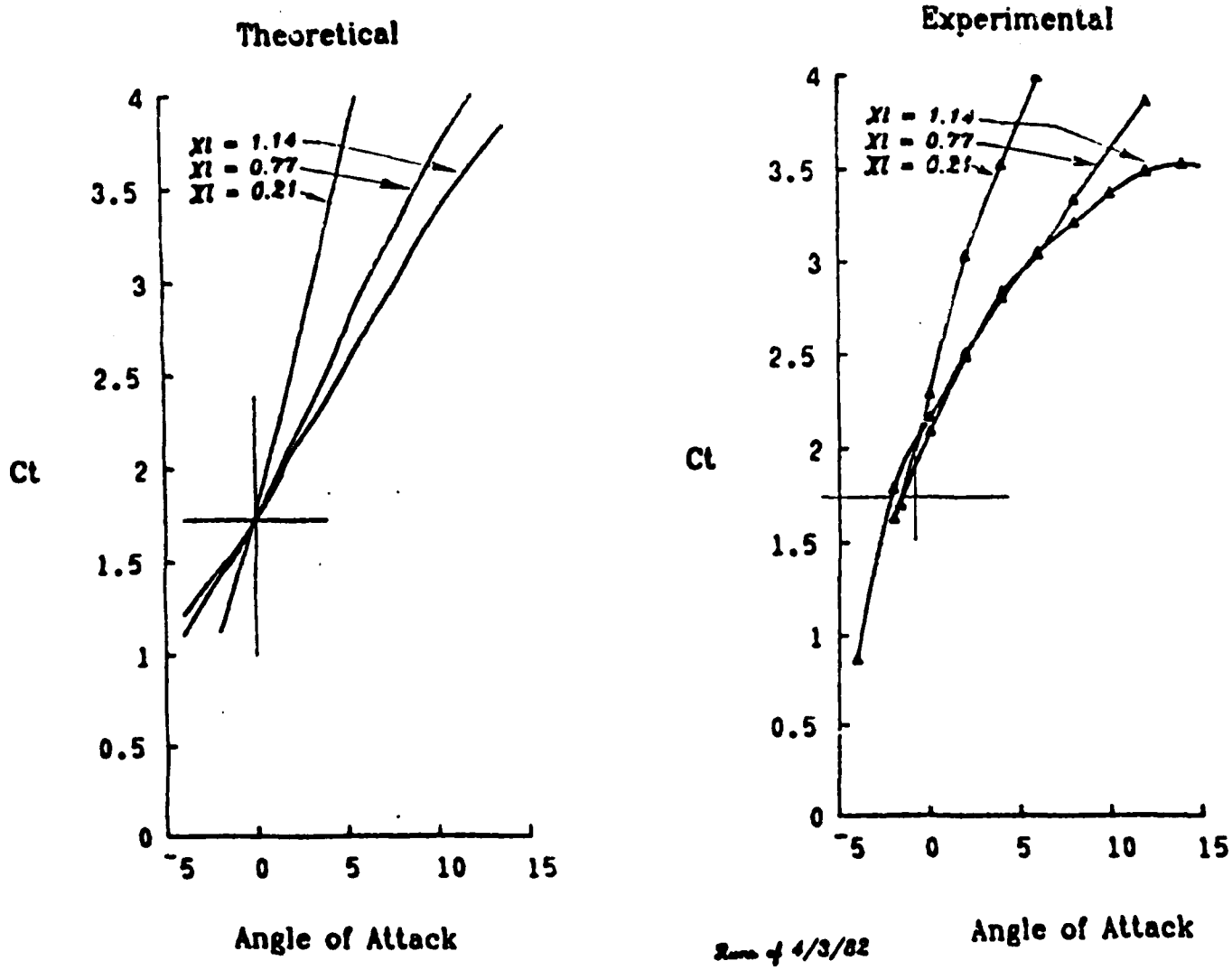

Figure 26. A Comparison of Theoretical and Experimental Tension Curves

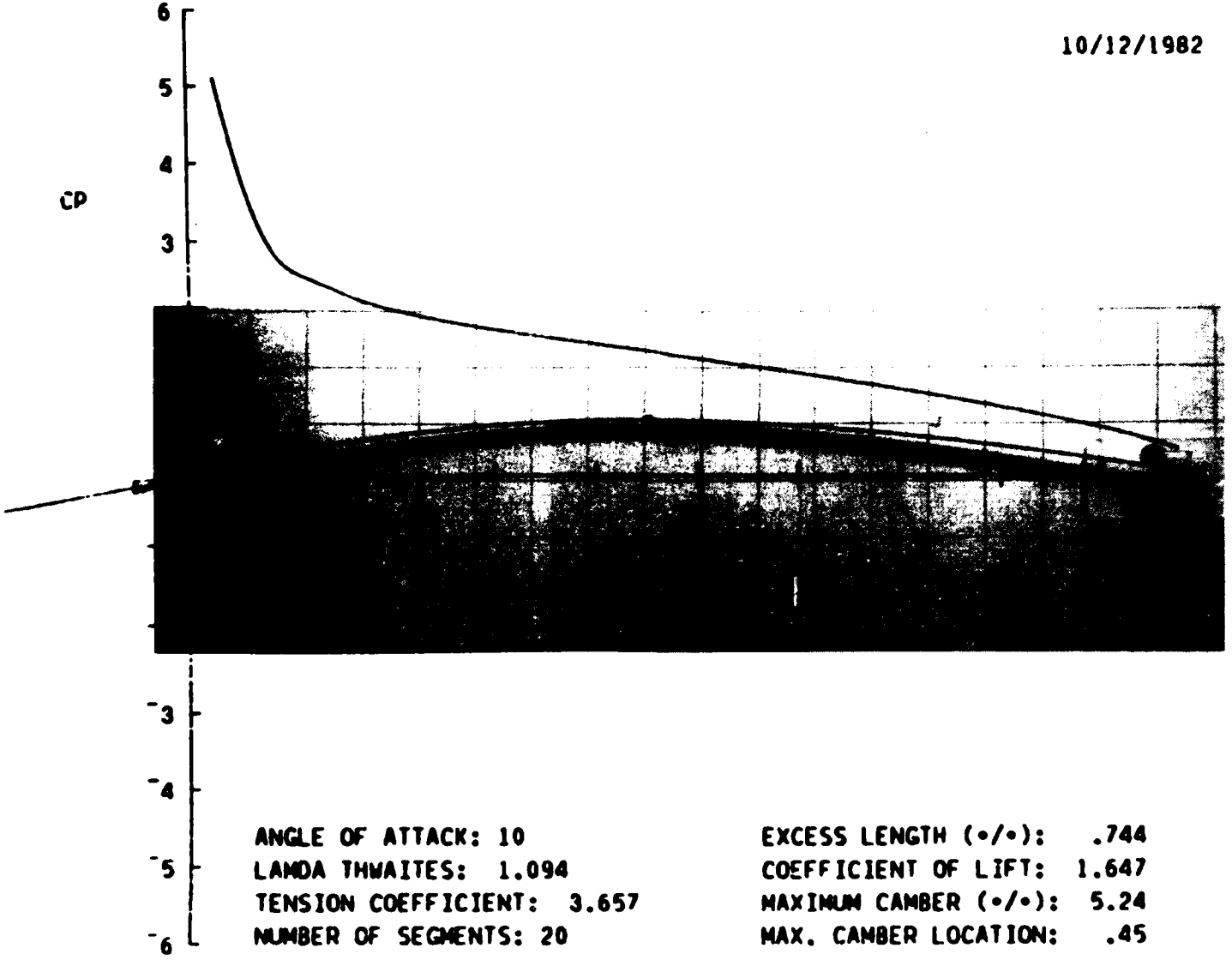

Figure 27. Membrane Shapes: A Comparison Between Theory and Experiment

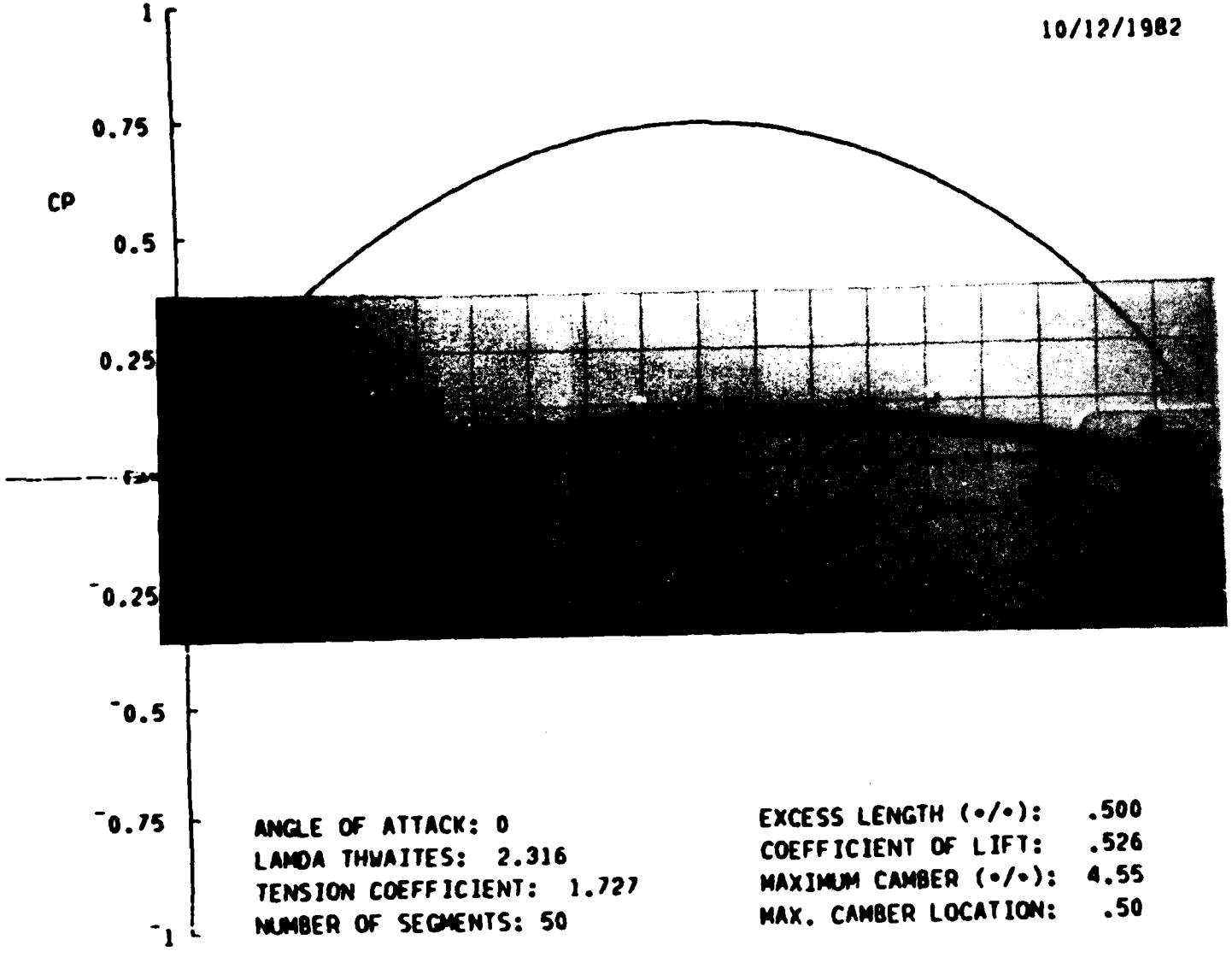

Figure 28. Membrane Shapes: A Comparison Between Theory and Experiment

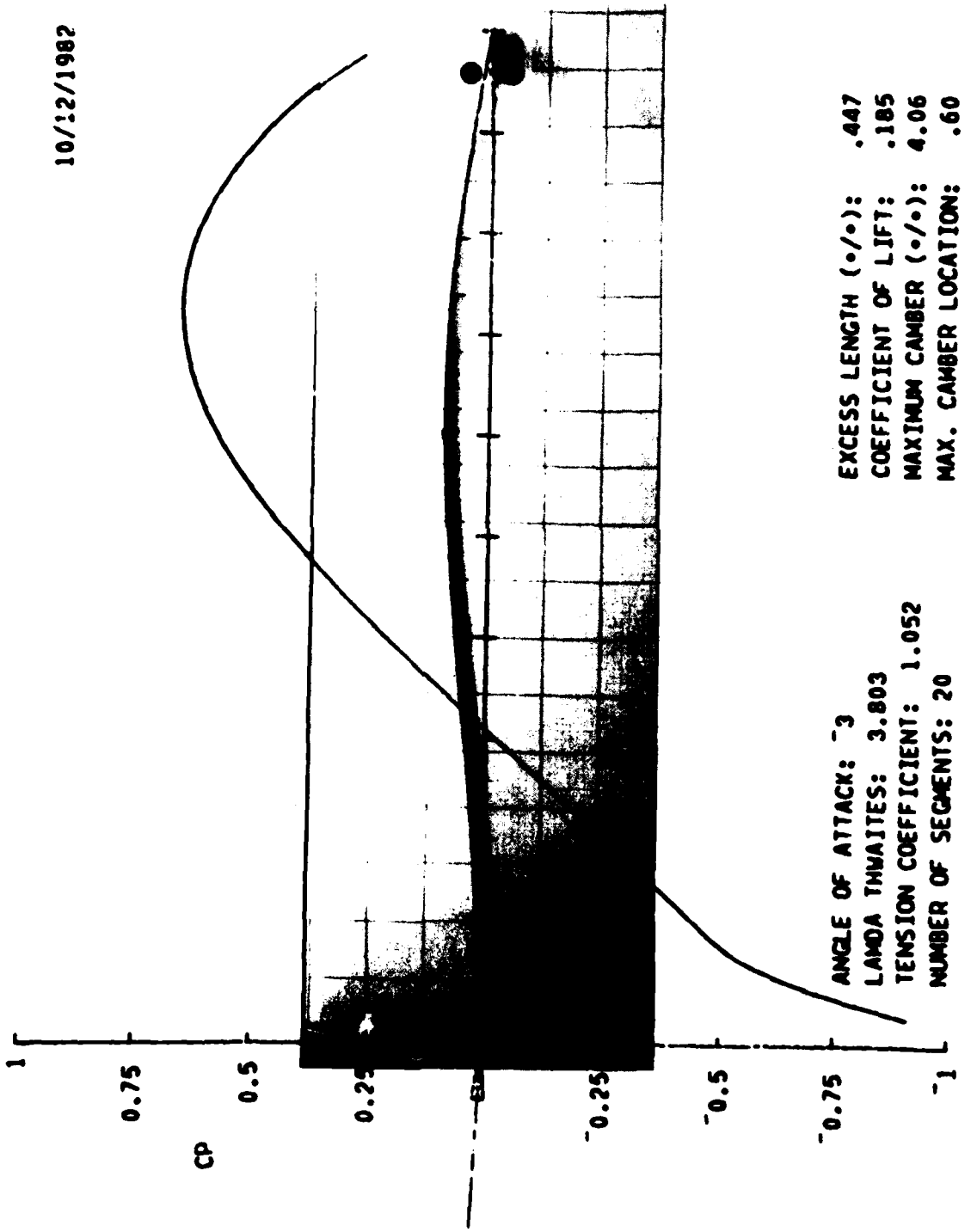

Figure 29. Membrane Shapes: A Comparison Between Theory and Experiment

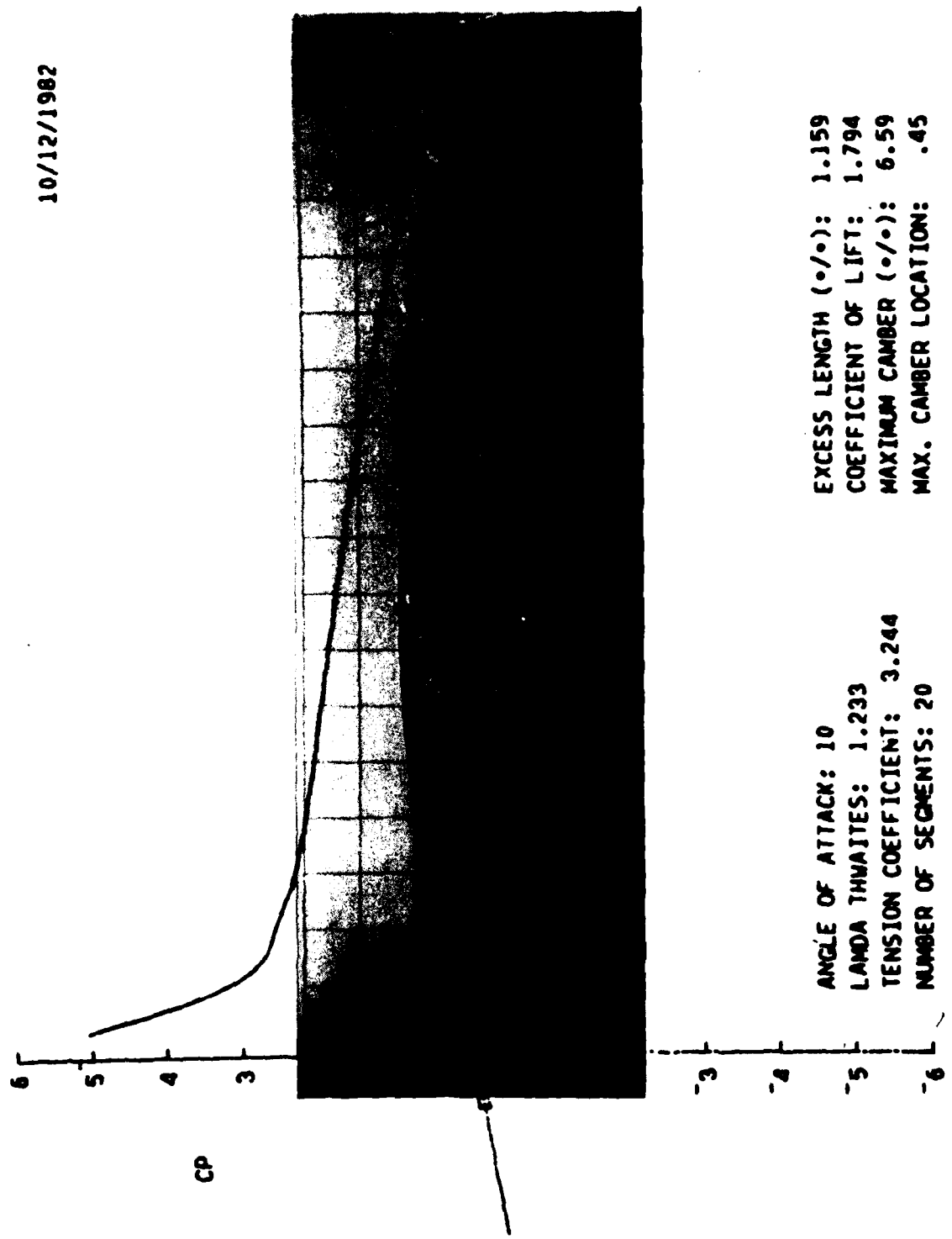

Figure 30. Membrane Shapes: A Comparison Between Theory and Experiment

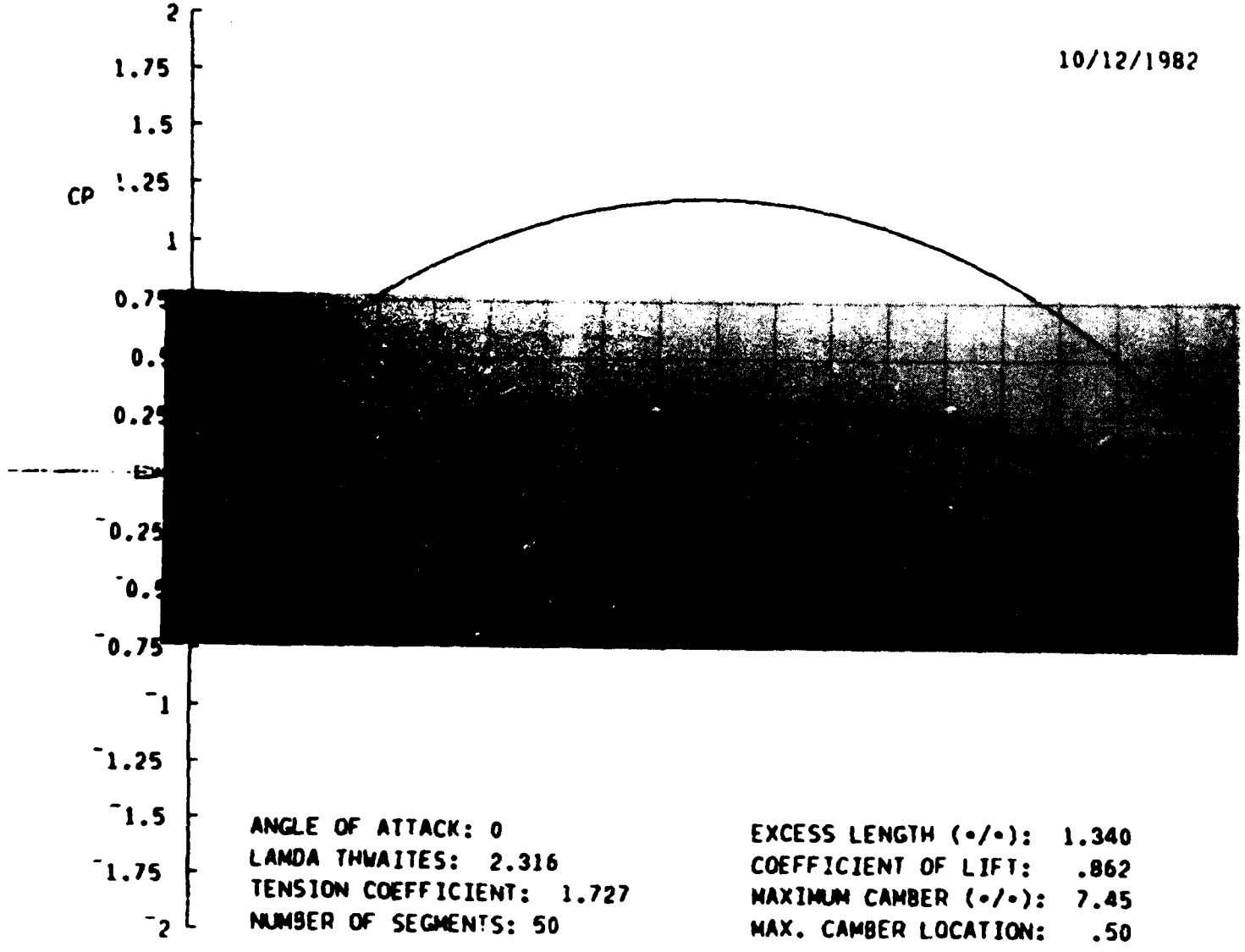

Figure 31. Membrane Shapes: A Comparison Between Theory and Experiment

NADC-83096-60

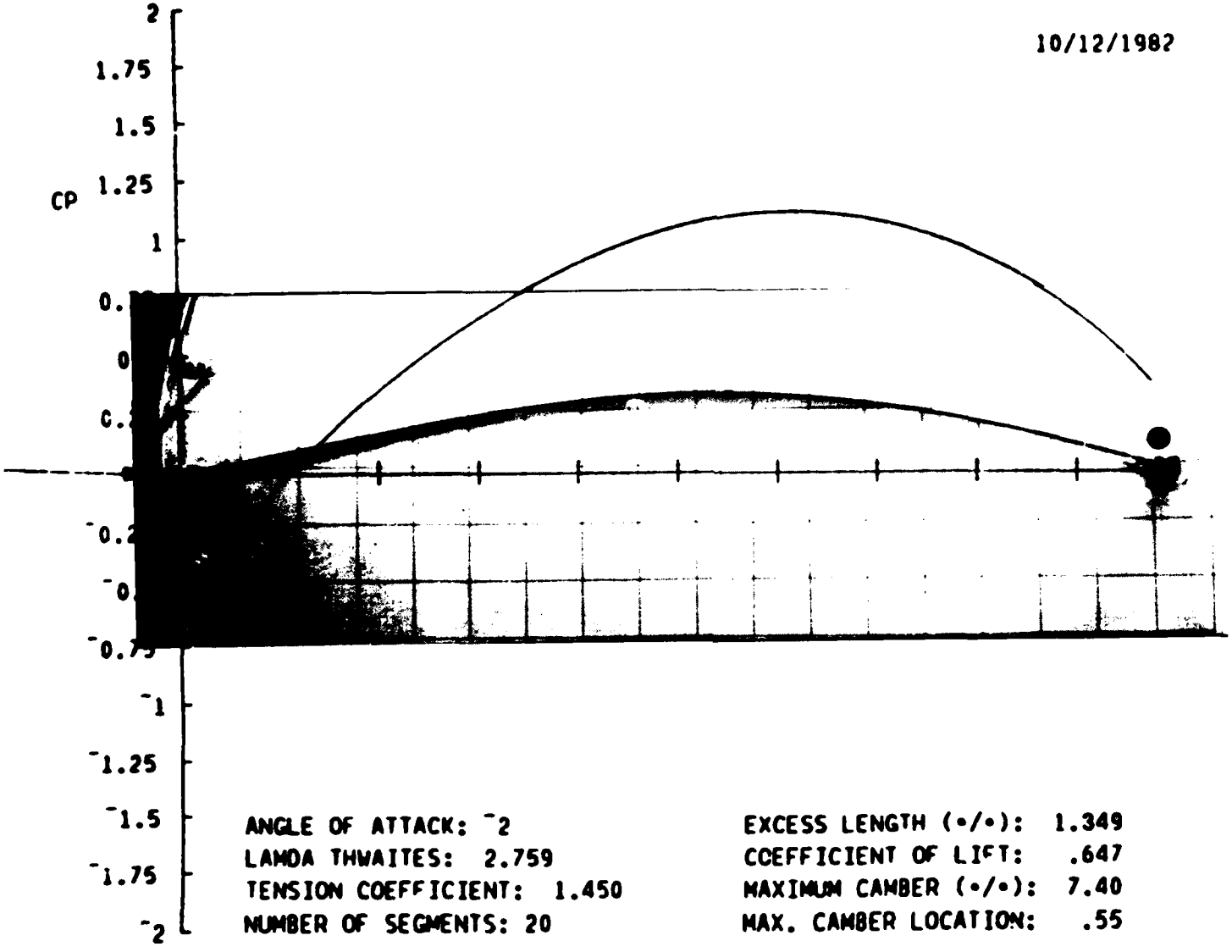

Figure 32. Membrane Shapes: A Comparison Between Theory and Experiment

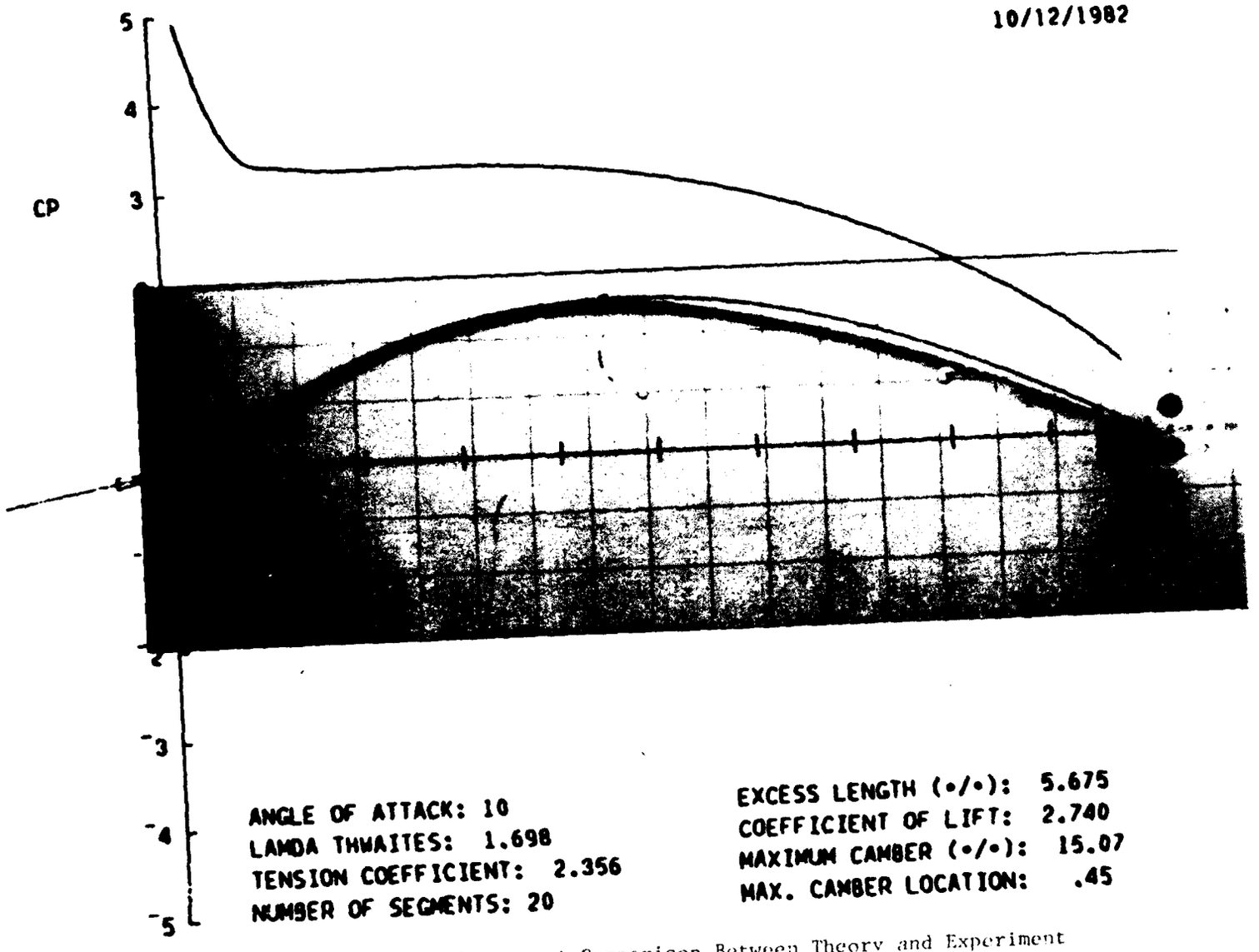

Figure 33. Membrane Shapes: A Comparison Between Theory and Experiment

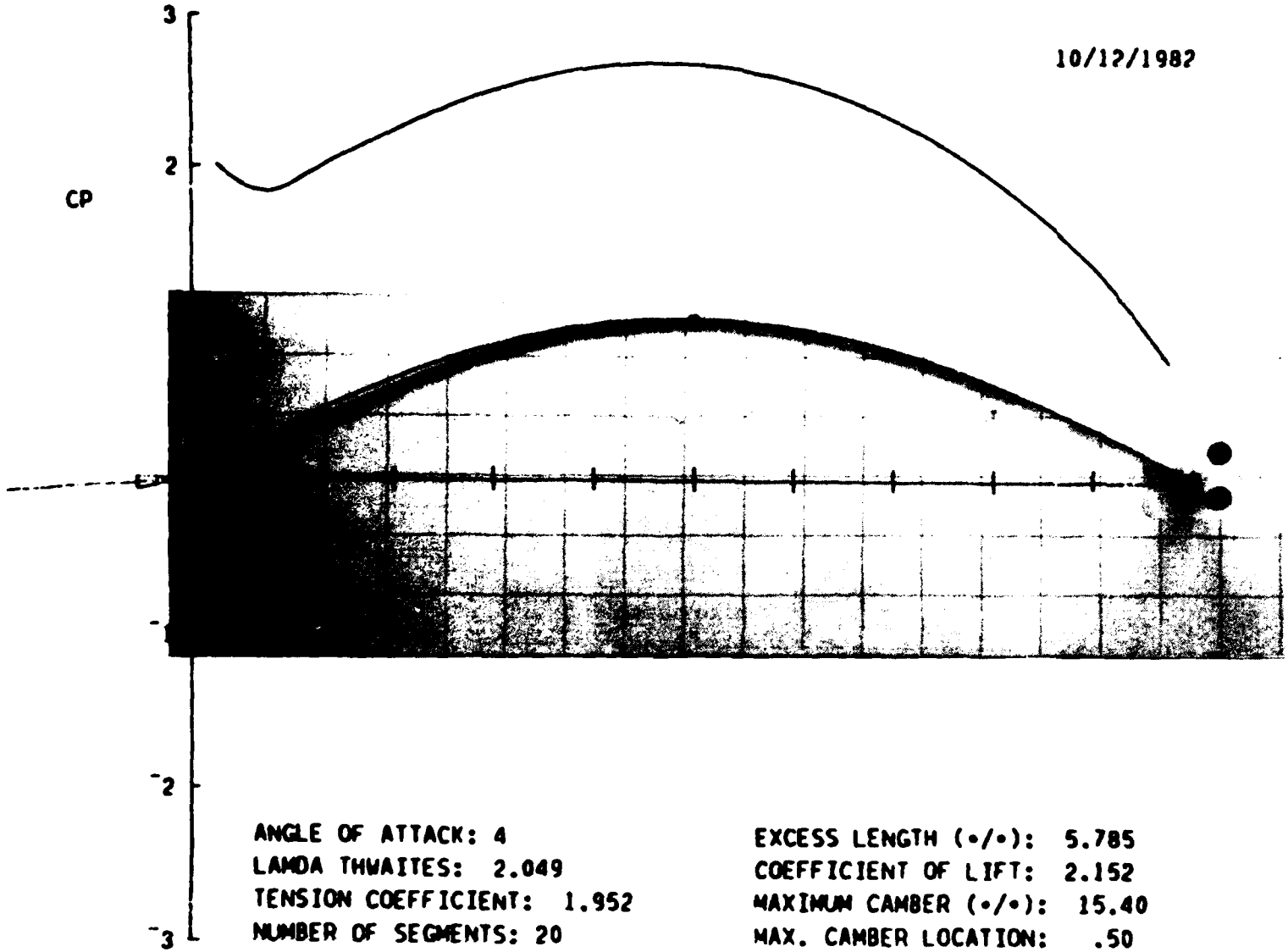

Figure 34. Membrane Shapes: A Comparison Between Theory and Experiment

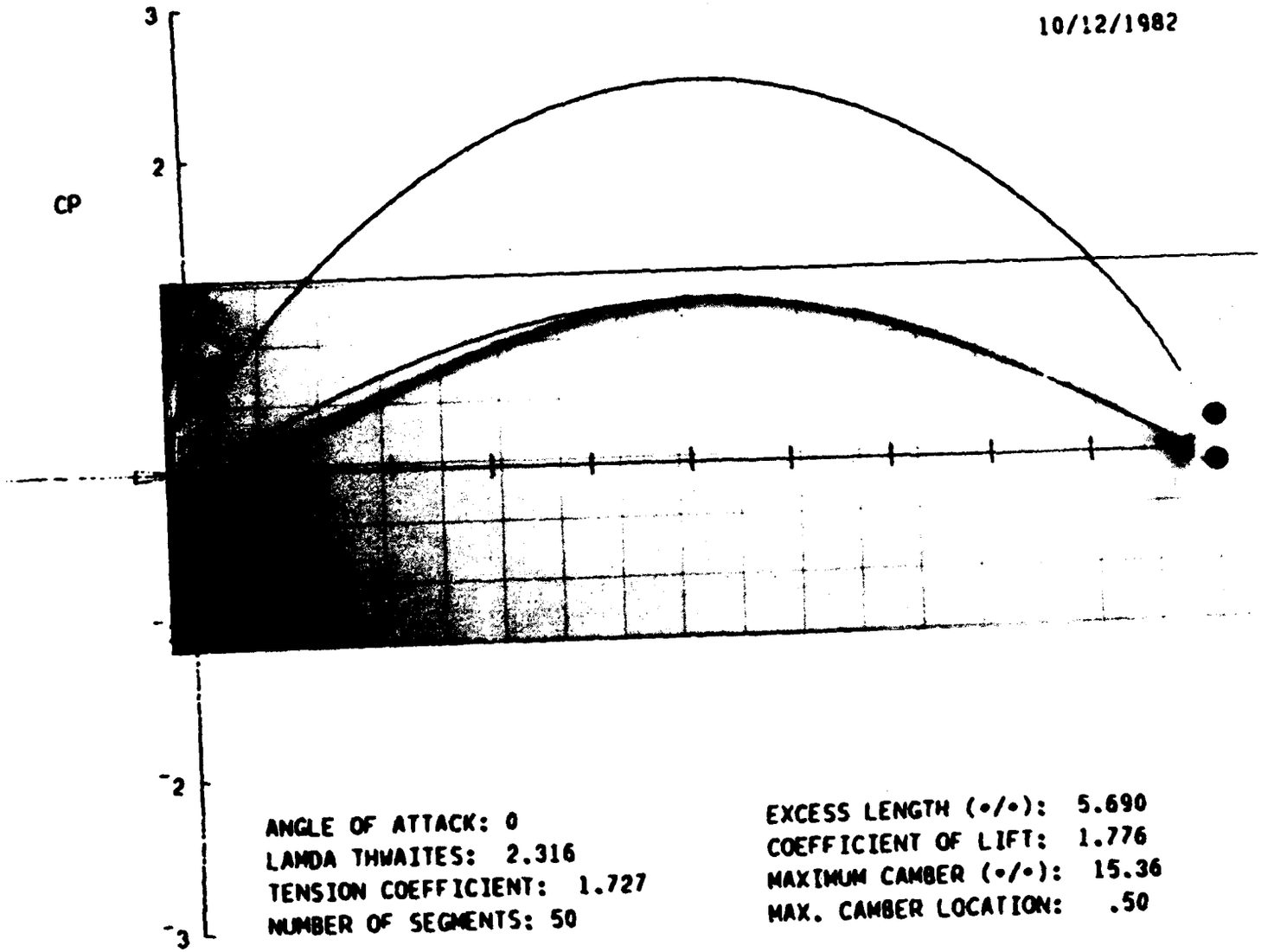

Figure 35. Membrane Shapes: A Comparison Between Theory and Experiment

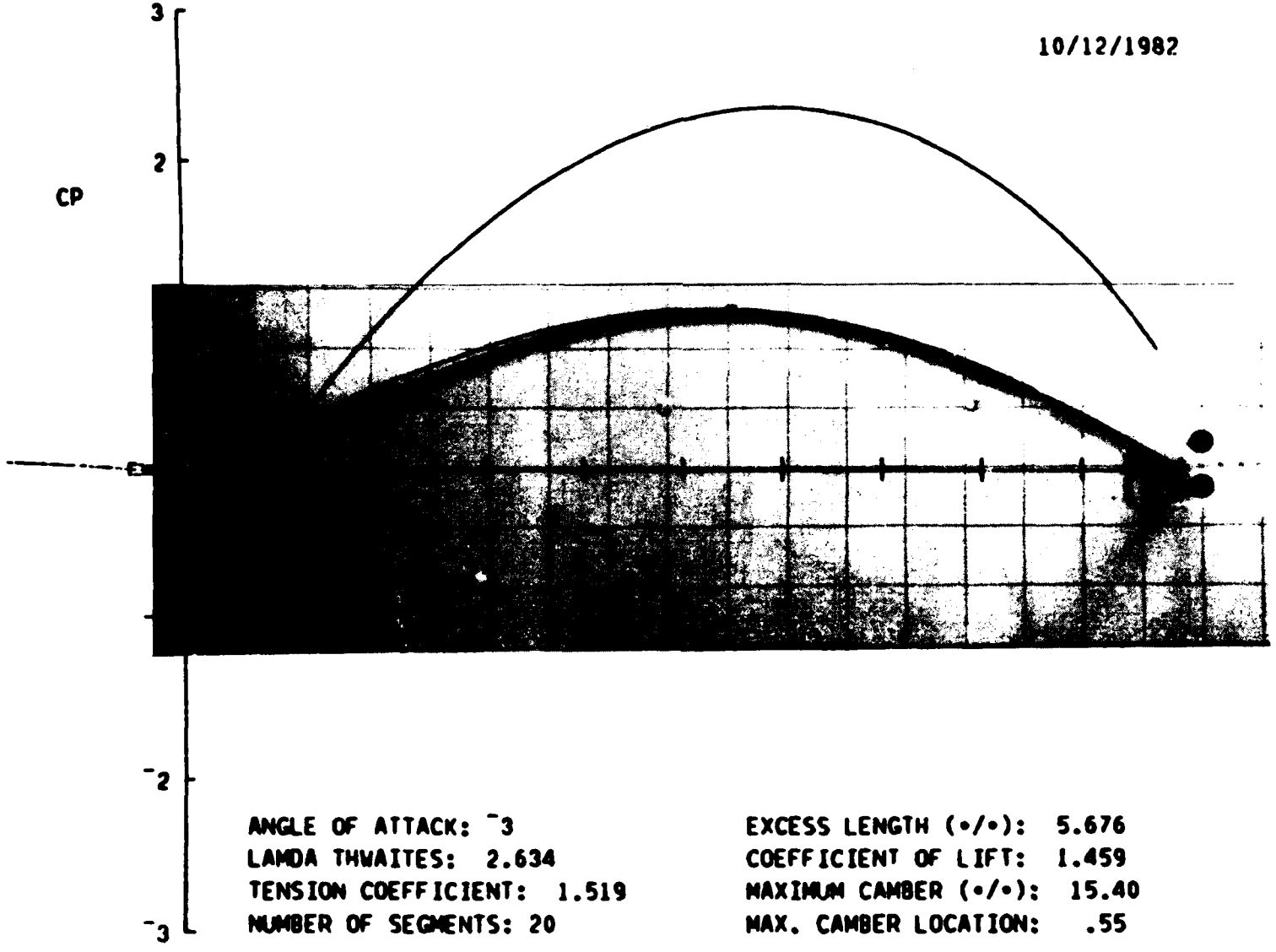

Figure 36. Membrane Shapes: A Comparison Between Theory and Experiment

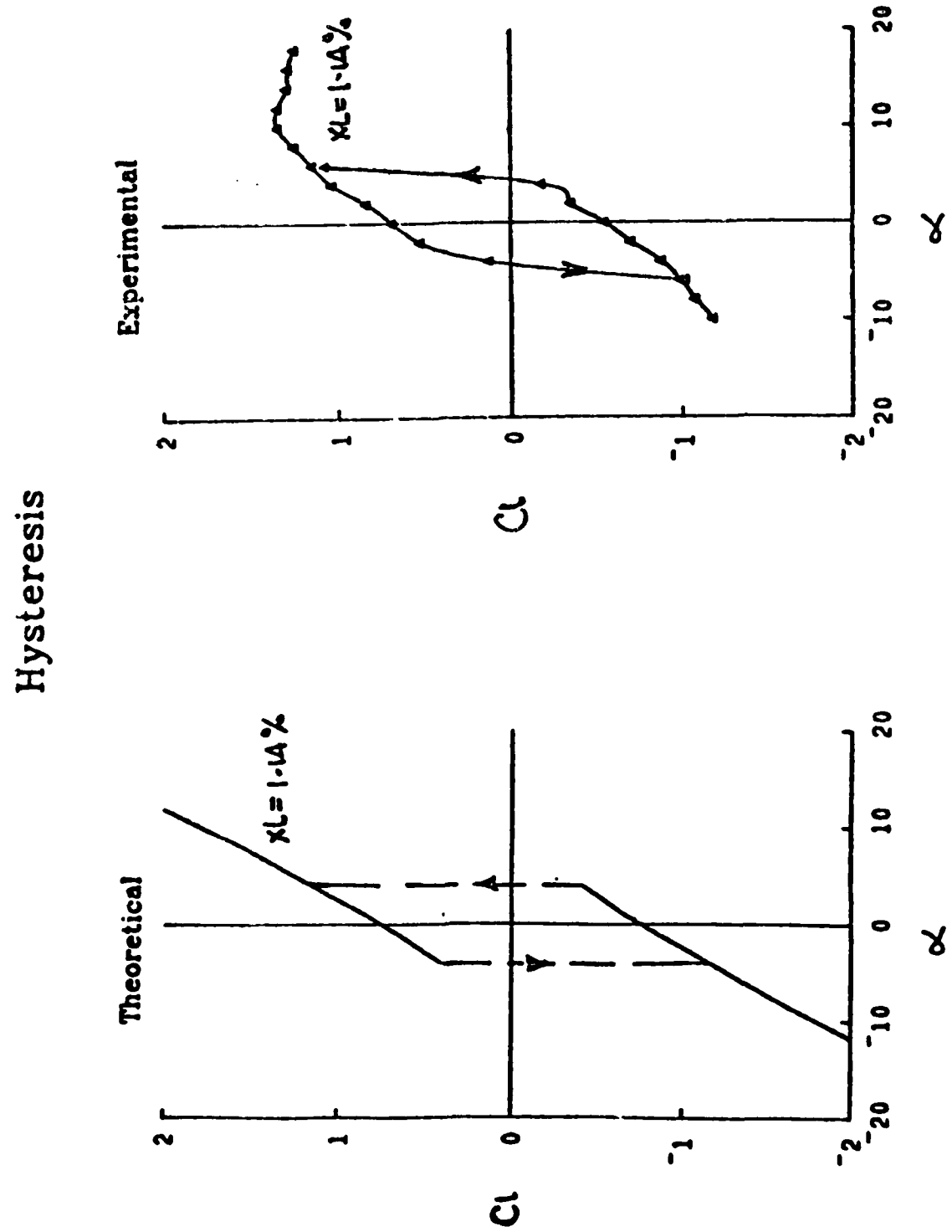

Figure 37. Theoretical and Experimental Lift Curve Hysteresis Loops

Hysteresis

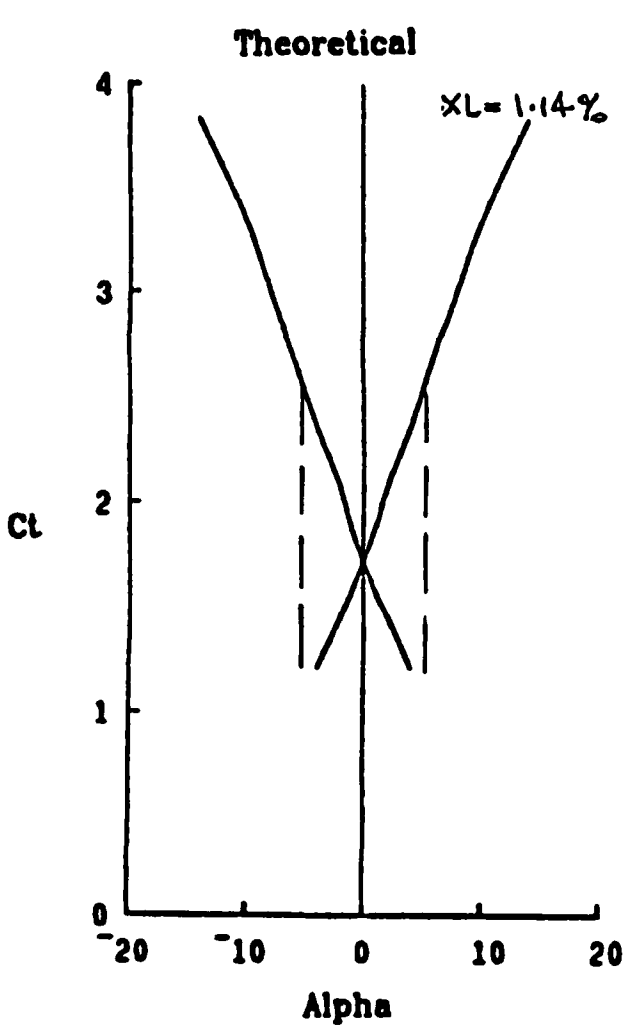

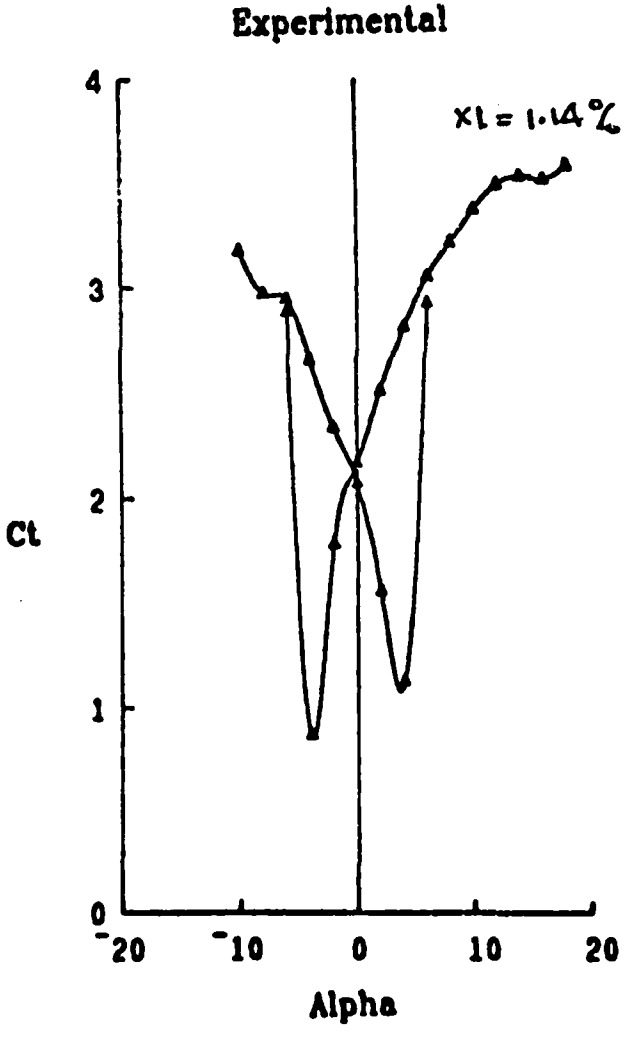

Figure 38. Theoretical and Experimental Tension Curve Hysteresis Loops

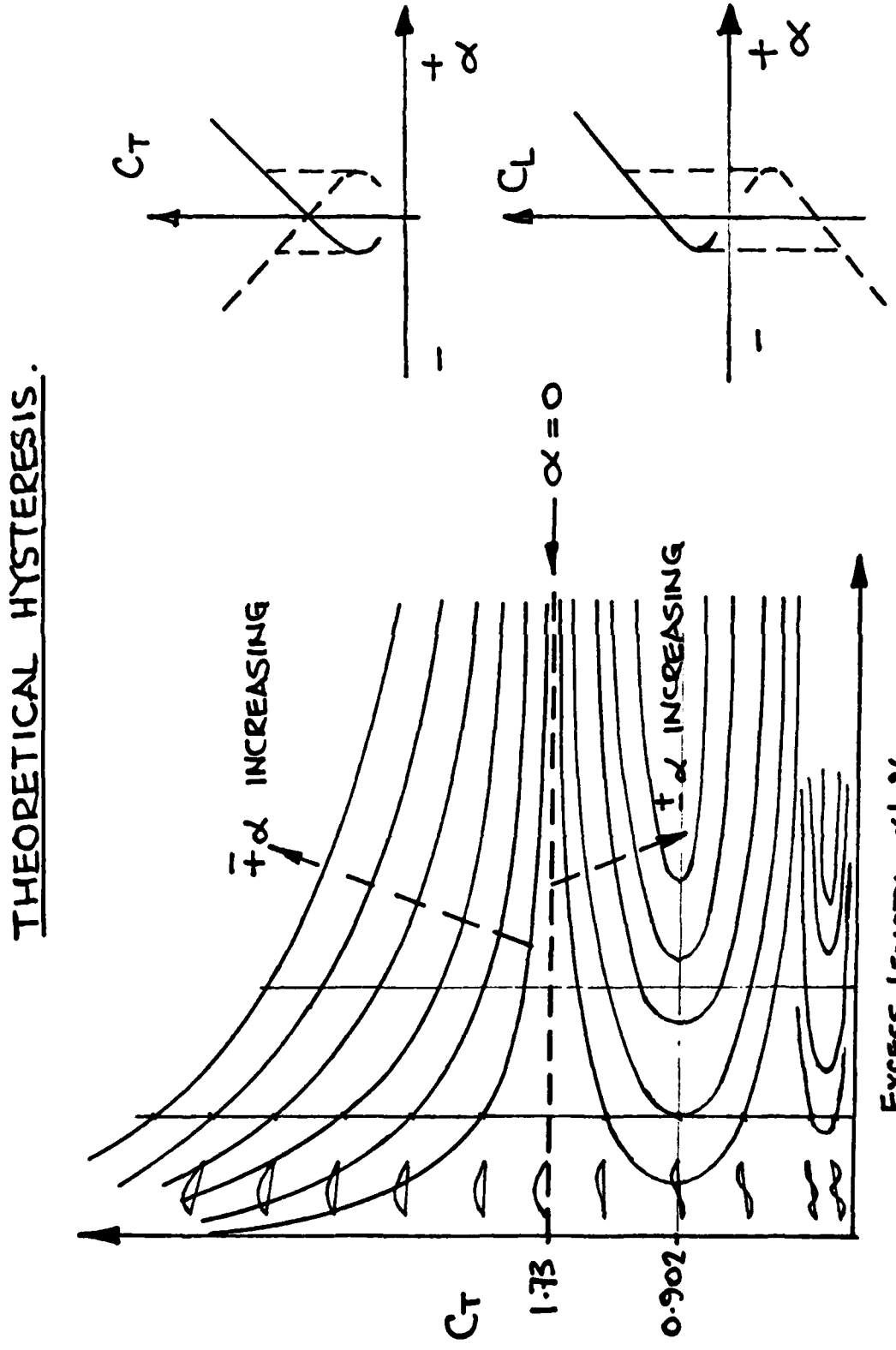

Figure 39. Coefficient of Tension vs Excess Length (Theoretical)

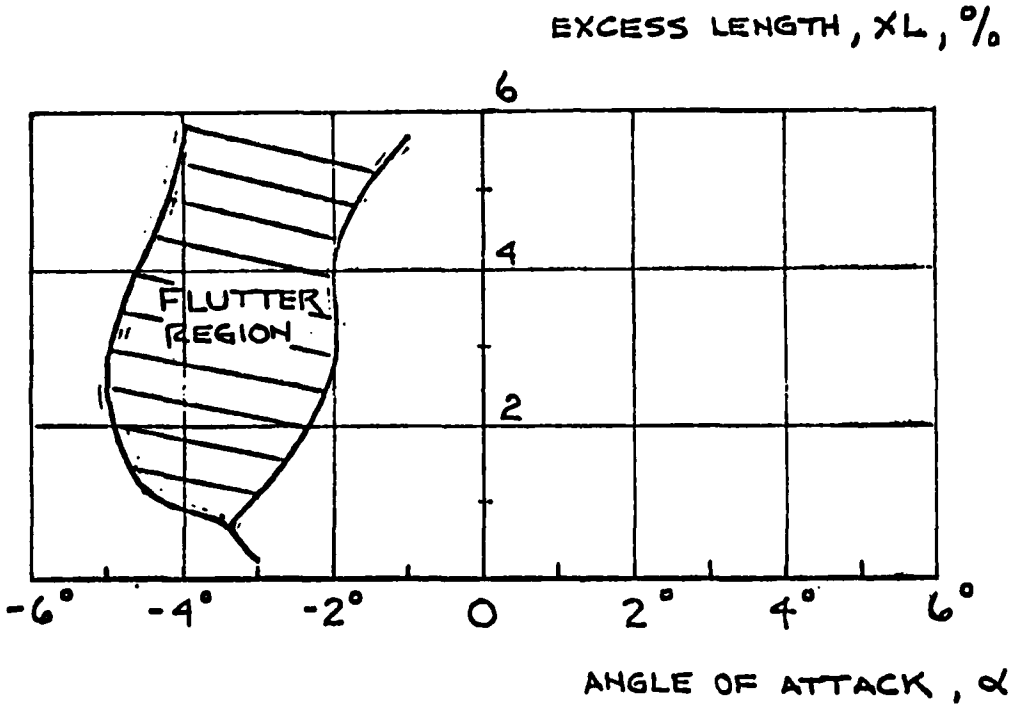

EXPERIMENTAL FLUTTER BOUNDARIES

EXCESS LENGTH VS. ANGLE OF ATTACK

Figure 40. Experimental Flutter Boundaries